공학석사 학위논문

Shear band evolution and deformation behavior of various metallic glass-forming alloys in bending mode

굽힘 변형 하에서 비정질 합금의

전단띠 형성 및 변형 거동 분석

2015 년 8 월

서울대학교 대학원

재료공학부

GHULAM YASEEN

Shear band evolution and deformation behavior of various metallic glass-forming alloys in bending mode

지도 교수 박 은 수

이 논문을 공학석사 학위논문으로 제출함
2015 년 8 월

서울대학교 대학원
재료공학부
GHULAM YASEEN

GHULAM YASEEN의 석사 학위논문을 인준함
2015 년 7 월

위 원 장 주 영 창 (인)

부위원장 박 은 수 (인)

위 원 한 홍 남 (인)

Abstract

Shear band evolution and deformation behavior of various metallic glass-forming alloys in bending mode

Ghulam Yaseen
Department of Materials Science and Engineering
The Graduate School
Seoul Nation University

In the present study we try to understand and characterize the shear band nature for various metallic glasses under different strain rates. We carefully evaluated the relationship between Kink angle (amount of plastic deformation) and estimated strain rates in various metallic glasses through the bend test of ribbon samples. The samples were bended between two platens in the bending machine with various platen speeds. After recovering curvature of ribbon sample the remaining kink angle of ribbon sample was measured by optical microscope. The different degree of kink angle is closely related to shear band density. For example, at higher estimated strain rate, less plastic deformation occurs, implied by smaller kink angle (fewer number of shear bands), while at lower estimated strain rate, higher plastic deformation occurs implied by

greater kink angle (higher number of shear bands) of the ribbon sample. The kink angles of various metallic glasses were also evaluated at same estimated strain rate. In relatively brittle metallic glass, deformed region is relatively small with local generation of shear bands with larger shear step height, while in relatively ductile metallic glass the deformed region is large with widely spaced shear bands with small shear step height. These results give us not only information on the deformation tendency depending on the deformation variables but also clues to understand the deformation mechanism of various metallic glasses.

Keywords: Metallic glasses, Kink angle, Strain rate, Shear bands, Deformation mechanism

Student Number: 2013-23812

Table of Contents

List of Figures

Figure 3.16. Load-deflection curve under 3-point bending test and SEM images of fractured surfaces, of as cast and annealed ($Zr_{52.5}Al_{10}Ti_5Cu_{17.9}Ni_{14.6}$) bulk metallic glass [35].

Figure 3.17. Load-displacement curve of as-cast ($Zr_{52.5}Al_{10}Ti_5Cu_{17.9}Ni_{14.6}$) bulk metallic glass at radius of 1.78 μm, represent the pop-in event and Hertzian solution [35].

Figure 3.18. Relation between cumulative probability vs τ_{max} at pop-in for as-cast and annealed samples at the radius of 1.8 μm [35].

Figure 3.19. The presence of soft zones in as-cast (a) and annealed ((b) half annealed, (c) fully annealed) samples [35].

Figure 3.20. (a) A representative load-displacement curve of $Fe_{79.3}B_{16.4}Si_4C_{0.3}$ metallic glass under nano-indentation at radius of 1.56 μm. (b) The relation between τ_{max} and cumulative probability for brittle ($Fe_{79.3}B_{16.4}Si_4C_{0.3}$) and ductile ($Zr_{50}Cu_{40}Al_{10}$) metallic glasses.

Figure 3.21. Shear band observation by SEM for brittle, $Fe_{79.3}B_{16.4}Si_4C_{0.3}$ (a) and ductile, $Zr_{50}Cu_{40}Al_{10}$ (b) metallic glasses after micro-indentation test at load of 200 gram.

Figure 3.22. Schematic diagrams and shear bands morphology of strong glass former ($Zr_{50}Cu_{40}Al_{10}$) at left side and fragile glass former ($Zr_{60}Cu_{30}Al_{10}$) at right side [19].

Figure 3.23. Relation between kink angle and estimated strain rate for strong metallic glass ($Zr_{50}Cu_{40}Al_{10}$) alloy and fragile metallic glass ($Zr_{60}Cu_{30}Al_{10}$) alloy under bending test.

Figure 3.24. SEM images of $Zr_{50}Cu_{40}Al_{10}$ (a) and $Zr_{60}Cu_{30}Al_{10}$ (b) metallic glasses, which measured at distance of 1.1 mm between plates with speed of 0.001 mm/sec of moving plate and it gives kink angle of 36.277^o for $Zr_{50}Cu_{40}Al_{10}$ (blue circle at figure 3.19) and 35.286^o for $Zr_{60}Cu_{30}Al_{10}$ (red circle at figure 3.19)metallic glasses.

Figure 3.35. Comparison of fatigue limit curve of $Cu_{46}Zr_{47-x}Al_7Y_x$ (x= 0, 5, 10) alloy series after bending fatigue test (as represented by dotted rectangle) and other Zr-based alloys [43].

List of Tables

Chapter 1. Introduction

1.1. Metallic glasses – development and applications

The searching for new and advanced materials with the passage of time is one of the main fascination of materials scientists. With the advance technology, recent investigation has been going on the improvement of existing materials or synthesizing of completely new materials. In recent years industrial development happened very rapidly when completely new materials have been synthesized that never heard before, among these metallic glasses, quasicrystals and high temperature superconductors are most commonly use now a days [1]. The materials that used before industrial revolution in the 18th century are mostly metals and these are limited to eleven kinds like gold, silver, iron, copper and etc [2]. A revolution from metals to metallic glasses happened when Pol Duwez in 1960, synthesized an Au-25 at.% Si alloy in the form of glassy state by rapidly solidifying the liquid at a rate 10^6 K/s [3]. Glass formation happened only when the generation of detectable crystal nuclei could be completely concealed, and it generally accepted that the volume fraction of these crystals is around 10^{-6}. In order to get glass formation the liquid should be cooled above the critical cooling rate (R_c), the concept of critical cooling rate can be easily explained with the help of figure 1.1 commonly known as T-T-T (time-temperature-transformation) diagram. In this diagram Y-axis represented the temperature, X-axis represented the time (logarithmic scale) while transformation curve which

helps to define the start of formation of crystals with the time at any given temperature is represented by C-shape. If the alloy is cooled at equilibrium condition (extremely low) from the liquid state (L_l) to solid state then solidification require a very long time and the final solidification product is always in crystalline state. Even if the liquid is solidified little rapidly as shown by curve 1 in figure 1.1, then the solidification takes place at temperature T_1 and time t_1 but the solidification product remains in crystalline state. But if the liquid is solidified at rate faster than critical cooling rate (curve 2 in figure 1.1) which is tangent to C-curve at its nose (represent the temperature at which formation of crystalline phase takes place at shortest time), the solidification product is always in glassy state. In this condition the liquid remains in the supercooled region (below T_g) and the final product is in glassy state. This T-T-T diagram helps to understand the nature of glassy phase and crystalline phase by considering solidification rate of liquid above or below to critical cooling rate [4]. A different techniques used in order to make metallic glasses depends upon the laboratories or sometimes a specific technique use for some special application/ production of metallic glass. Some of the techniques; high-pressure die casing, water quenching, copper mold casting, arc melting, are most commonly used in order to make metallic glasses. These techniques are used to make bulk metallic glasses having section thickness of at-least few millimeters, while in order to make metallic glass ribbons (having thickness of few micrometers), rapid solidification processing (RSP) technique use commonly. The cooling rate of different

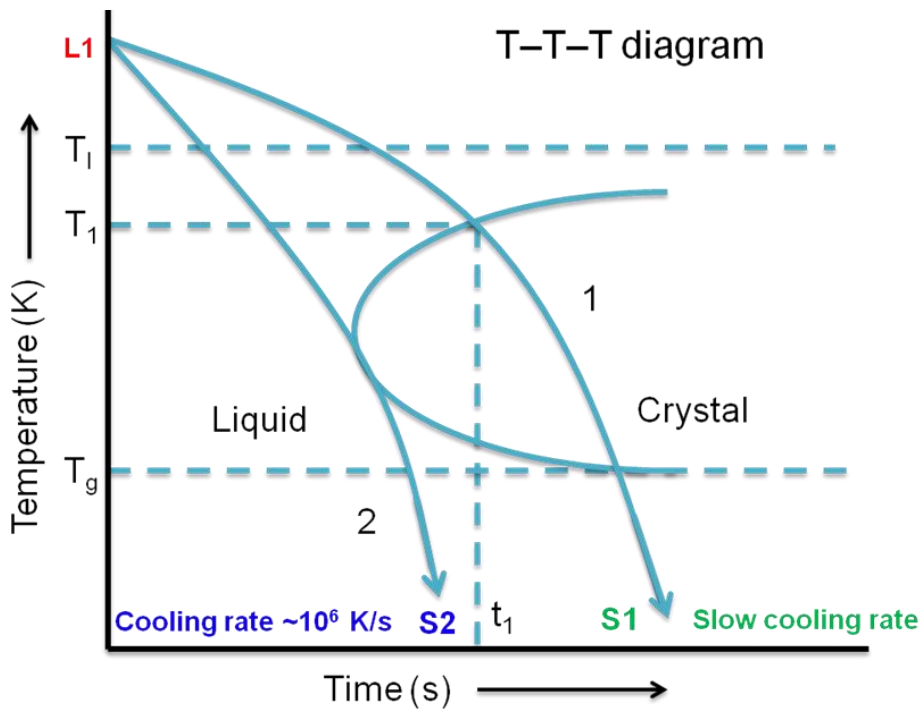

Figure 1.1. T-T-T diagram for the alloy system [4].

technique is different from each other but the cooling rate of each technique is higher than critical cooling rate which helps to produce metallic glasses in the form of glass state whether bulk metallic glasses or metallic glass ribbons [5-7]. Glass forming ability (glassy state) of metallic glasses depends on the composition, cooling rate and other factors.

Because of glassy state nature bulk metallic glasses exhibit very high strength, very high hardness, excellent corrosion resistance and a good combination of soft magnetic properties. One of the big advantages of bulk metallic glasses is the ease of formation at different shapes. Bulk metallic glasses having casting diameter more than 1 cm, are summarize in table 1.1 with their specific properties, these are using for the development of innovative products for industrial applications. Because of very high strength of bulk metallic glasses, they have widespread applications in sporting goods like golf clubs (figure 1.2), tennis rackets, bicycle parts, fishing applications, marine applications and etc. Bulk metallic glasses are using to make spring for cars that are slimmer and make themselves shorter because of low young modulus of bulk metallic glasses. The usage of these valve springs in engine, reduces the internal volume and make the engine lighter which helps in fuel consumption (figure 1.2) [8]. Similarly bulk metallic glasses are using in defense and space exploration applications because of their high specific strength (figure 1.2). Light weight, high strength and excellent wear resistance of bulk metallic glasses are make them to use in daily products like laptops and hand wrist watches (figure 1.2) [9]. One of the latest industries attracted by bulk metallic glasses is the

Composition (at. %)	D_c (mm)	Reported Properties	Published Year
$Pd_{40}Ni_{40}P_{20}$	25	High fracture strength (1700 MPa)	1996
$Pd_{40}Cu_{30}Ni_{10}P_{20}$	72	High fracture strength (1680 MPa)	1996
$Pt_{57.5}Cu_{14.7}Ni_{5.3}P_{22.5}$	12	High fracture strength (1470 MPa) Compressive ductility (20%)	2004
$Pd_{35}Pt_{15}Cu_{30}P_{20}$	30	High fracture strength (1410 Mpa)	2006
$Mg_{56}Cu_{26.5}Ag_{8.5}Gd_{11}$	25	High fracture strength (1000 MPa)	2005
$Co_{48}Cr_{15}Mo_{14}C_{15}B_6Tm_2$	10	High fracture strength (4000 MPa) Nonmagnetic	2006
$Ni_{50}Pd_{30}P_{20}$	21	High fracture strength (1780 MPa) Compressive ductility	2007
$Cu_{46}Zr_{42}Al_7Y_5$	10	None mentioned	2004
$Cu_{44.25}Zr_{36}Ti_5Ag_{14.75}$	10	High fracture strength (1970 MPa)	2006
$Cu_{40}Zr_{44}Ag_8Al_8$	15	High fracture strength (1850 MPa) Compressive ductility	2006

Table 1.1. Typical bulk metallic glasses having casting diameter more than 1 cm into fully glassy forms [8].

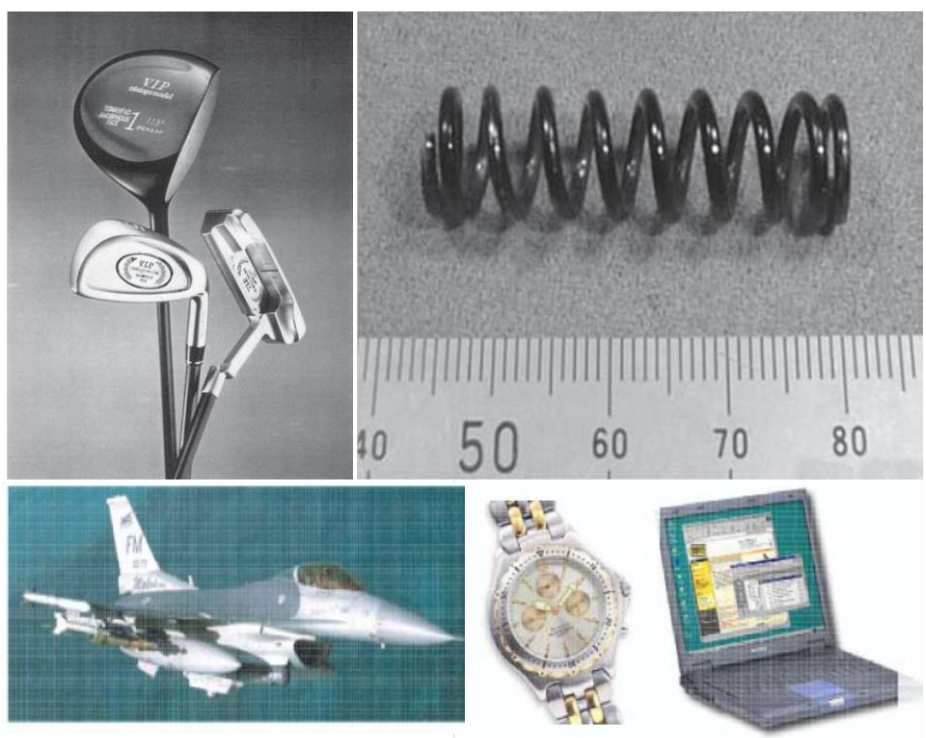

Figure 1.2. Applications of bulk metallic glasses in different fields [8, 9].

jewelry industry due to their stunning surface finish, which attain the attention of jewelry makers worldwide. Due to the easiness of bulk metallic glasses for the casting in different shapes as compared to other metals, also enables jewelry designers to concentrate on it. It belief that in the near future bulk metallic glasses hold the materials dealing not even in research but also in industrial applications [10].

1.2. Structural inhomogeneity of metallic glasses

1.2.1. Free volume in strong and fragile metallic glasses

By Angell, the liquids can be classified into strong and fragile liquids (glass formers) [11]. Strong glass formers have good glass forming ability and they are highly viscous, while fragile glass formers have only marginal glass forming ability with low viscosity. A glass forming ability parameter helps to understand the difference between strong and fragile glass formers. A glass forming ability parameter,F_1 is

$$F_1 = 2\left[\frac{m}{m_{min}}\left(\frac{1}{T_{rg}-1}\right) + 2\right]^{-1}$$

Where m is fragility index, $m=m_{min}$ shows higher fragility and T_{rg} is reduced glass transition temperature. As can noted that the value of F_1 changes with T_{rg}, R_c and m. The glass forming ability increases with the increase of T_{rg} and

with the decrease of R_c and m. The value of F_1 is around zero for fragile liquids, while its value is $2T_{rg}/(1+T_{rg})$ for strong liquids. An exponential relation between R_c and F_1 identified by plotting F_1 as a function of R_c, as can see below;

$$R_c = R_{co}\, e^{(-AF_1)}$$

Where R_{co} is 2.7 x 10^{11} Ks^{-1} and A is 48.7. As explained above, for fragile liquid (F_1=0), R_c = 2.7 x 10^{11} Ks^{-1}, which is in good agreement with the critical cooling rate for producing of pure metals in glassy state. While in case of strong liquid T_{rg} = 2/3 (F_1=0.8), R_c = 2.3 x 10^{-6} Ks^{-1}, which is comparable to critical cooling rate required for the producing of SiO_2 [12]. By using the same approach Zheng analyze the relaxation time for Mg-Cu(Ag)-Gd alloys and reported the formation of bulk metallic glasses with the critical diameter around 20-27 mm [13].

1.2.2. Secondary phase in phase separating metallic glasses

Some as-solidified glassy rods (especially binary bulk metallic glasses) contains very fine crystals (nano-meter dimensions) which dispersed in glassy matrix. The existence of these crystals are due to the low glass forming ability of alloy. For example, if the sample contains a crystalline phase then may be the critical cooling rate is not exceeding through-out the cross section of

sample and the resulting matrix contains glassy and crystalline phases. Sometimes as-solidified samples contain crystalline particles on the surface due to occurrence of heterogeneous nucleation on the surface of sample or with those parts that are in contact with metallic substrate. Also the primary crystallization sometimes occurs with solid solution phase in a glassy matrix due to heating of the glassy samples at higher temperatures [14]. It noted that some alloys shows phase separation in which two glassy phases are present which is different from above case. Phase separation happened during the process of solidification in the supercooled region or during reheating of homogenous glassy phase. Phase separation occurrence happened for those alloy systems whose phase diagram features a miscibility gap between two phases that are thermodynamically stable. This is common for the alloy systems that have zero or positive heat of mixing among the at-least two constituent elements. It also occurs for those alloys that have negative heat of mixing among the constituent elements but in this case it's very rare. Figure 1.3 shows the schematic diagram which featuring the miscibility gap, in this figure T_1 is temperature at which alloy is in single liquid phase while T_2 is quenched temperature which passes through miscibility gap. If an liquid alloy at T_1 is quenched to T_2 in the miscibility gap and it has composition between C_1 and C_2, then it is in a meta-stable high energy state and it lower its free energy by decomposing into two phases. The lowest energy of this meta-stable solid solution is obtained when it decomposes into C_1 and C_2 solid phases. But if the liquid is quenched from T_1 to T_2, and it lies between $C_{1'}$ and $C_{2'}$,

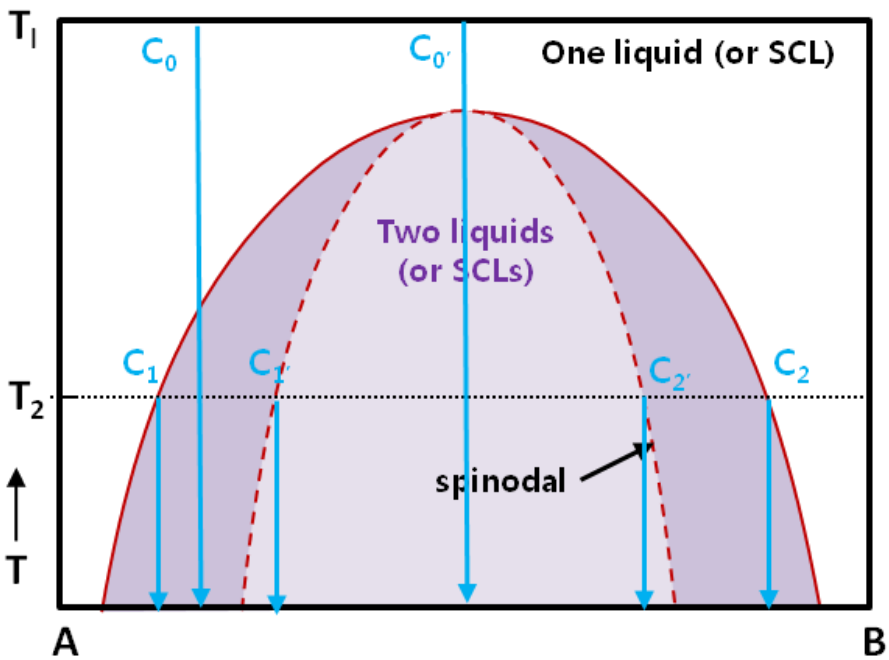

Figure 1.3. Phase diagram for phase separated metallic glass showing the miscibility gap in the solid state [15].

then it is in highly unstable state and any small changes in composition let the decrease of free energy of the system. Such type of transformation is called spinodal transformation. It noted that phase separation decomposition of supersaturated solution occurs either by a nucleation and growth process (which need to overcome the nucleation barrier) which lies between C_1 and C_2 as in below figure 1.3 (point C_o), or by a spinodal process which lies between $C_{1'}$ and $C_{2'}$ in figure 1.3 (point $C_{o'}$) and which doesn't have any nucleation barrier [15]. Chen and Turnbull noticed that the phase separation occurred in Pd-Si and Pd-M-Si alloys even they have negative heat of mixing among the constituent elements [16]. Phase separation of Cu-Zr-Al-Y alloy series was noticed due to positive heat of mixing of Zr-Y (+35 KJ/mol) elements [17].

1.3. Plastic deformation in metallic glasses

As explained in section 1.1, metallic glasses have amorphous nature (non-crystalline structure) and this cause the much intention for the understanding of deformation behavior of metallic glasses. It's very long time known that deformation in crystalline materials happened due to sliding of blocks of the crystals (periodic arrangement of atoms) on each other along definite crystallographic planes which called slip planes [18]. While in case of metallic glasses the exact deformation behavior is still unknown but there is a general agreement that deformation in metallic

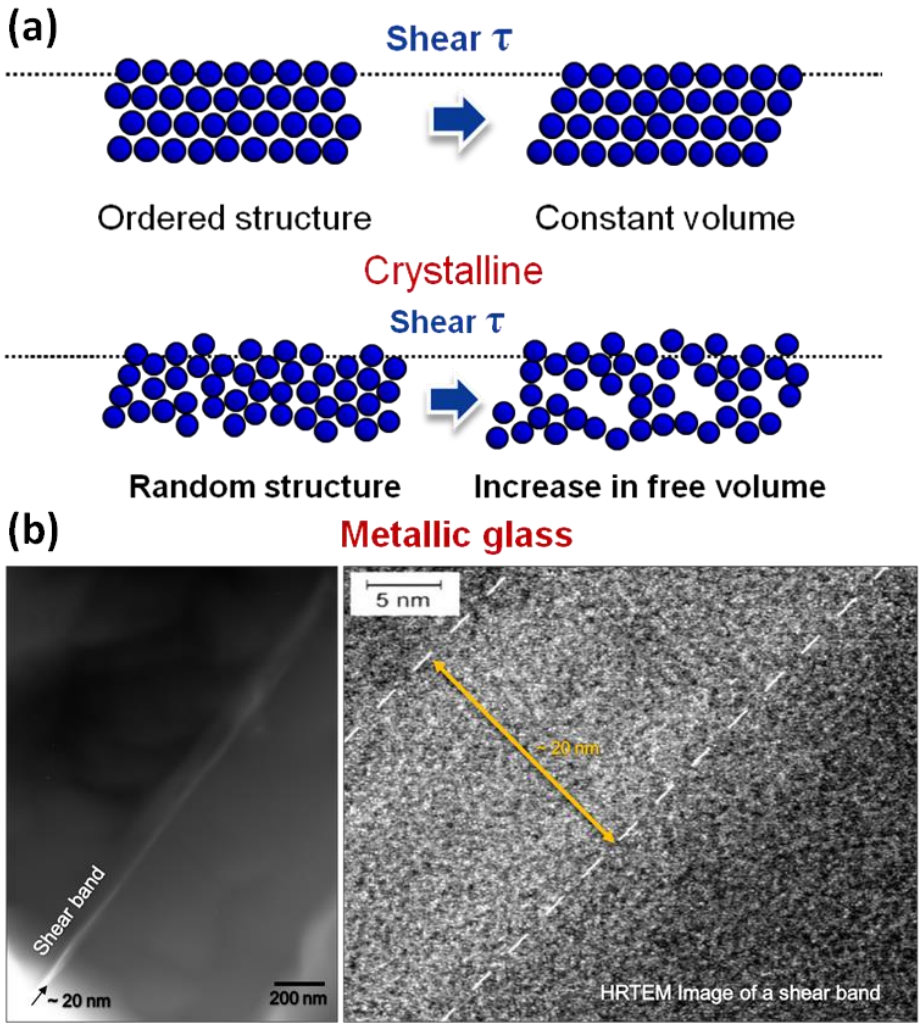

Figure 1.4. (a) Deformation behavior in crystalline materials (top image) and in metallic glasses (below image) due to dislocation and free volume creation respectively. (b) Shear band observation in metallic glass under TEM (left side) and magnified image of shear band (right side) [19].

glasses occurred due to atomic rearrangement that accommodates shear strain. Due to amorphous nature of metallic glasses, the deformation takes place at higher shear strength as compared to crystalline materials. Because crystalline materials, dislocations occurred under shear strength, while in case of amorphous materials, atomic rearrangement happened under shear strength which cause dilation (creation of free volume) in metallic glass as shown in figure 1.4 (a). Because of free volume creation, shear band initiated in metallic glass which cause the permanent deformation in metallic glass. Figure 1.4 (b) shows shear band observation under transmission electronic microscope (TEM). The magnified image of shear band clearly shows the less contrast area as compared to non-shear band area due to free volume creation [19].

1.4. Research Objective

The drawback of metallic glasses is their brittle nature as compared to conventional metals. Metallic glasses show very high engineering stress as compared to conventional metals but metallic glasses don't show any plasticity as compared to conventional metals which have very high engineering strain. Due to few shear bands generation or one major shear band generation in metallic glasses cause the brittle fracture. A comparative relation between engineering stress versus engineering strain for metallic glass and conventional metal shown in figure 1.5. The fracture surface of metallic glass shows mirror like feature which is the indication of brittle

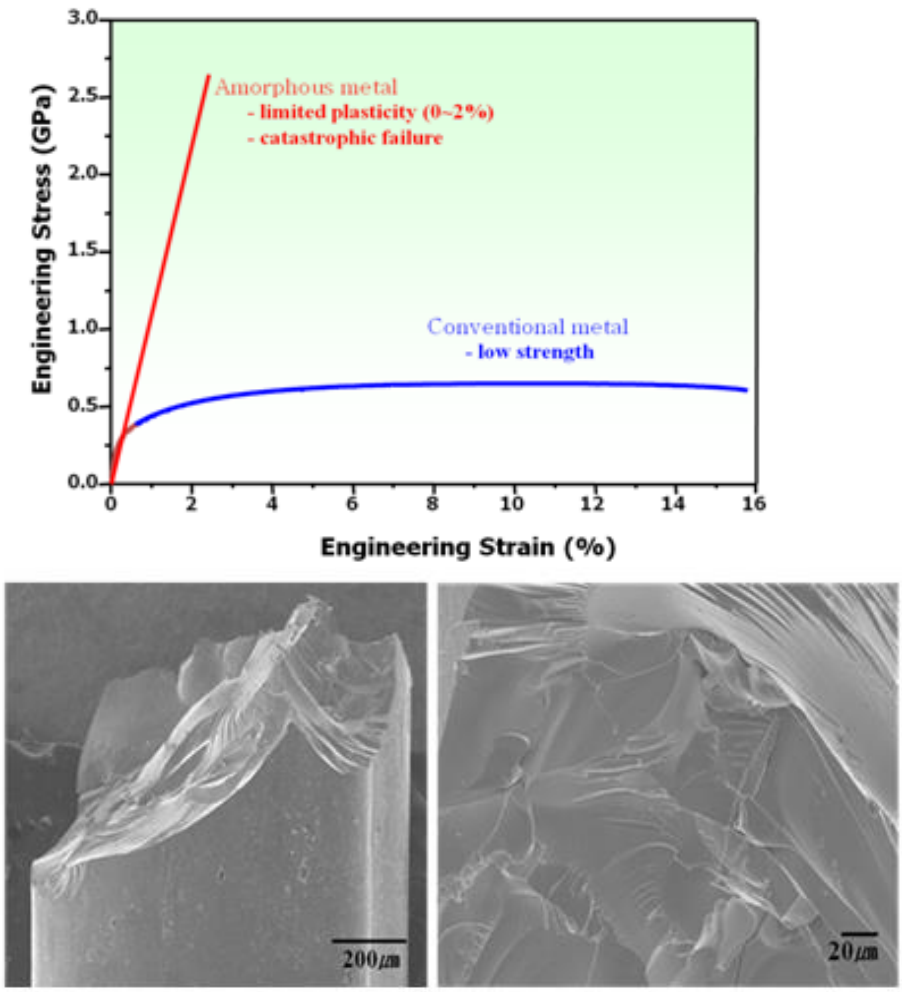

Figure 1.5. Comparative relation between engineering stress versus engineering strain for metallic glass and conventional metal. The fracture surface of metallic glass shows mirror like feature which is the indication of brittle fracture [20].

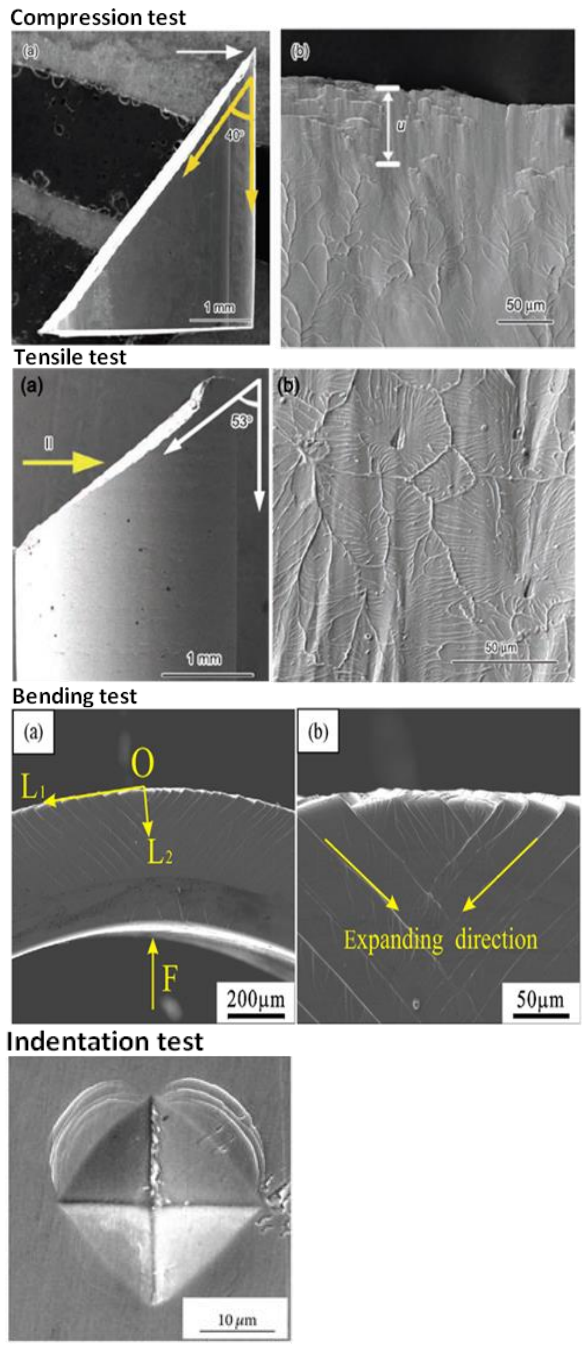

Figure 1.6. Shear bands observation of bulk metallic glasses under various mechanical tests [21-23].

fracture [20].

Different mechanical tests are used in order to observe deformation behavior (shear band morphology) of bulk metallic glasses, like compression test, tensile test, bending test, indentation test and etc. as shown in figure 1.6. It can be noted that few or no shear band (except vein pattern on fractured surface) observed normally under compression or tensile test of bulk metallic glasses but shear bands clearly observed under bending and indentation tests [21-23]. The major problem of bulk metallic glasses is their processing and many metallic glasses exhibit low glass forming ability in a bulk form.

In order to more clear understanding of deformation behavior of metallic glasses, metallic glass ribbons were widely used. Metallic glass ribbons can be easily prepared by melt spinning process which has cooling rate around 10^6 K/s. A melt spinning diagram shown in figure 1.7, while the process explained in section 2.1. Under tensile test of ribbon samples, it's very difficult to observe shear bands while the fracture surface only shows the vein pattern as can see in figure 1.8 [24]. Figure 1.8 shows SEM images of fracture surfaces from ribbons ($Ni_{40}Ta_{35}Co_{20}Nb_5$ on left, $Ni_{30}Ta_{35}Co_{30}Nb_5$ on right) tested in tension. As compared to tensile test, under indentation test shear bands more clearly observed around indenter, but in this case the shear band morphology is similar for different metallic glasses as shown in figure 1.8 [25, 26]. Figure 1.8 shows SEM images of the indents of the $Cu_{60}Zr_{20}Ti_{20}$ and $Cu_{50}Al_{30}Mg_5Ti_{15}$ alloys, which shows different number of scale pile shear bands around indenter but the morphology of shear bands is

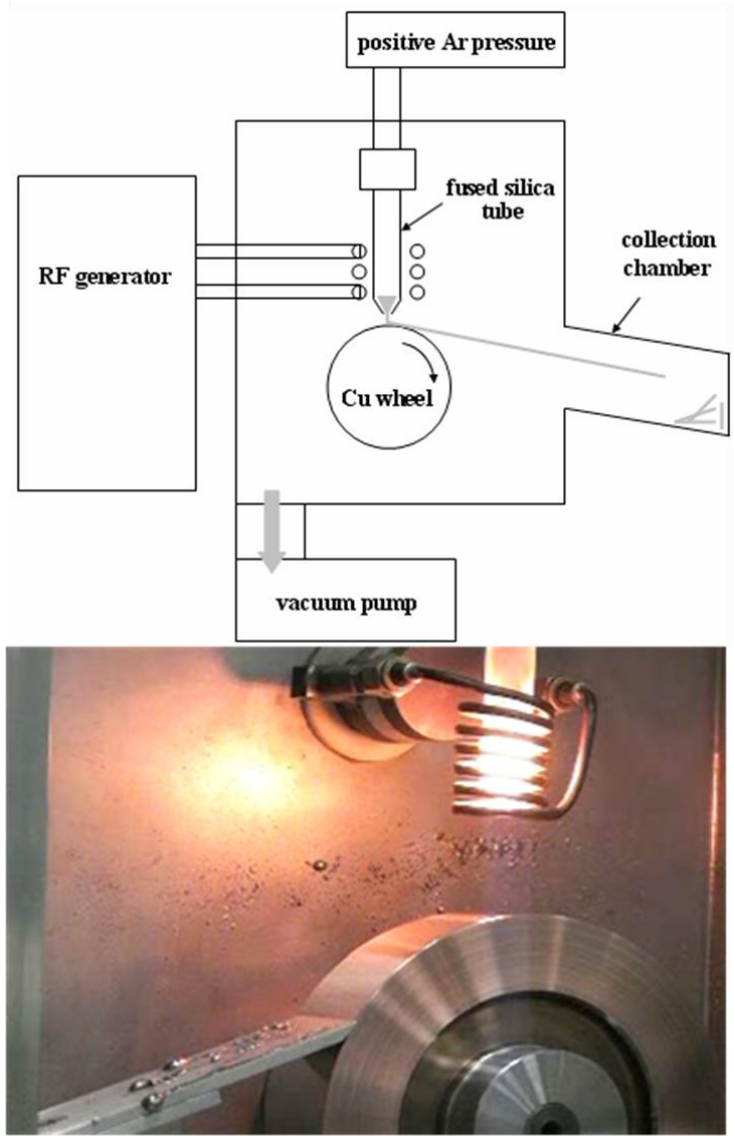

Figure 1.7. Fabrication of metallic glass ribbon in melt-spinning process.

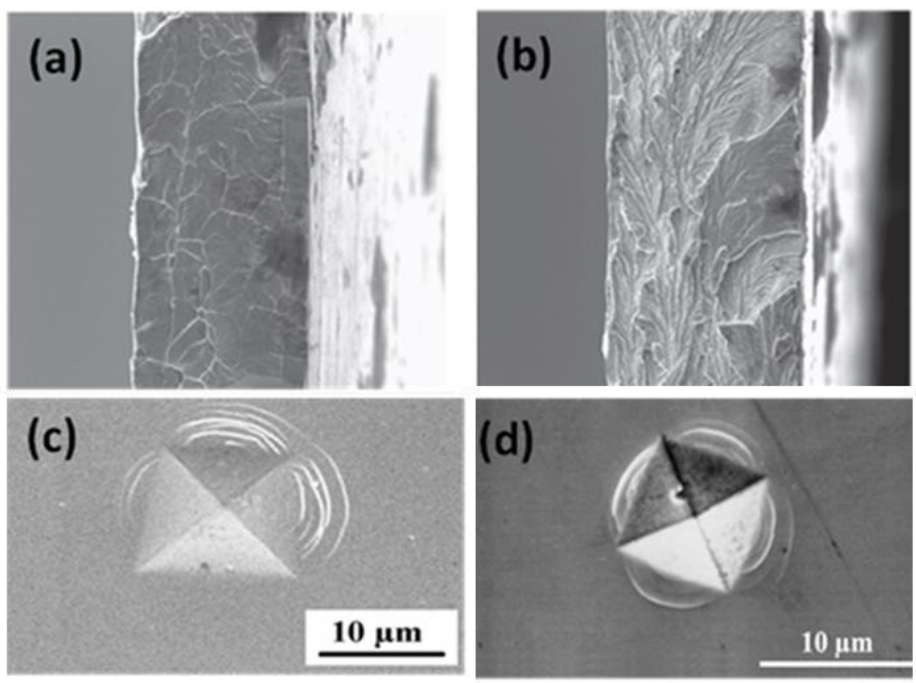

Figure 1.8. SEM images of fracture surfaces from ribbons ($Ni_{40}Ta_{35}Co_{20}Nb_5$ (a), $Ni_{30}Ta_{35}Co_{30}Nb_5$ (b)) tested in tension. SEM image of the indents of the $Cu_{60}Zr_{20}Ti_{20}$ (c) and $Cu_{50}Al_{30}Mg_5Ti_{15}$ (d) alloys [24-26].

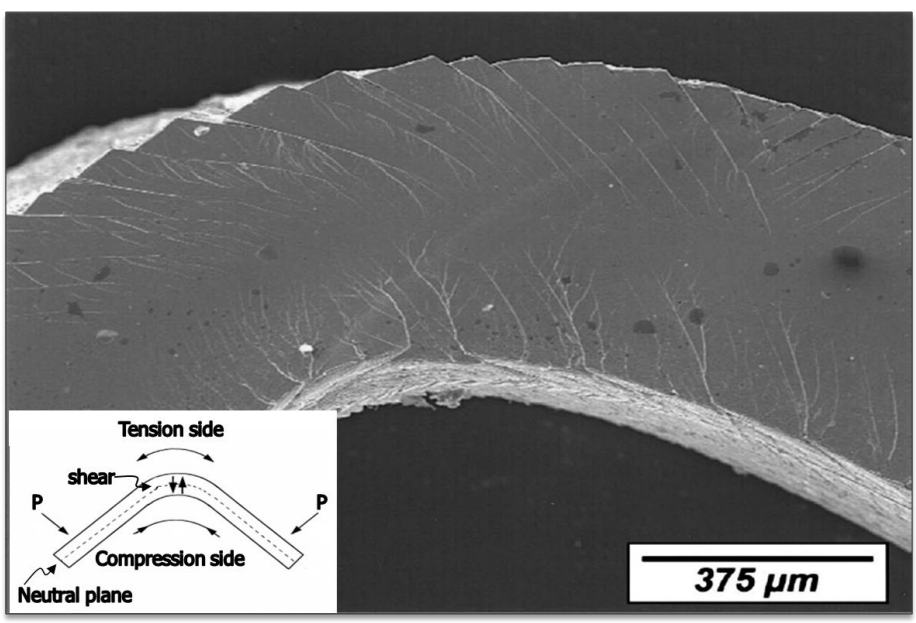

Figure 1.9. Shear bands evolution in metallic glass ribbon by bending deformation [27].

same that is semi-circular shear bands at four sides of indenter for both alloys. But under bending test of metallic glass ribbons we can more clearly observed shear bands at tension and compression side as shown in figure 1.9 [27].

By considering the major issue of metallic glasses that is deformation behavior of metallic glasses, in this research I tried to explain the deformation behavior of different metallic glasses which have different mechanical properties like yield strength and different structural characterization like high/low free volume or free volume/scale heterogeneity by using bending test. Bending test was applied to brittle ($Fe_{79.3}B_{16.4}Si_4C_{0.3}$)/ ductile ($Zr_{50}Cu_{40}Al_{10}$), strong glass former ($Zr_{50}Cu_{40}Al_{10}$)/ fragile glass former ($Zr_{60}Cu_{30}Al_{10}$) and monolithic ($Cu_{46}Zr_{47}Al_7$)/ non-monolithic ($Cu_{46}Zr_{42}Al_7Y_5$, $Cu_{46}Zr_{37}Al_7Y_{10}$) metallic glass ribbons. Ribbon samples of each composition were prepared by melt spinning process which has similar thickness and width. Bending test was applied at different experimental conditions (like different speed between plates or different distance between plates), in order to know the effect of experimental variation on each metallic glass ribbon sample and also the results of different composition alloys compare with each other. Deformation region (shear bands) of all metallic glass ribbons were observed after bending test (at specific condition for each case) with the help of scanning electronic microscopy. Dynamic observation of shear bands of brittle ($Fe_{79.3}B_{16.4}Si_4C_{0.3}$) and ductile ($Zr_{50}Cu_{40}Al_{10}$) metallic glasses helps to know the shear band kinetics of these two compositions. Shear bands morphology of these metallic glass ribbons were also observed under

scanning electronic microscopy after micro-indentation test at different loads. Nano-indentation test was used in order to know the structural in-homogeneity of each metallic glass ribbon by considering the maximum shear strength at pop-in point (initiation of shear band/ permanent deformation point).

Chapter 2. Experimental Procedure

2.1. Sample preparation

In this study different kinds of metallic glass ribbon samples were used. Monolithic multi-component $Zr_{50}Cu_{40}Al_{10}$, $Zr_{60}Cu_{30}Al_{10}$, $Zr_{47}Cu_{46}Al_7$ and non monolithic multi-component $Cu_{46}Zr_{42}Al_7Y_5$, $Cu_{46}Zr_{37}Al_7Y_{10}$ alloy ingots with weight of ~20gram, were prepared by arc melting with appropriate amounts of high purity Zr (99.95%), Cu (99.99%), Al (99.95%) and Y (99.95%) under Ti-gettered argon atmosphere. The constituent elements of the alloy ingot after weight and clean from ethanol were put on the water cooled copper hearth, which then evacuated and backfilled by highly pure Argon gas after closing the chamber. In order to reduce oxygen contamination, pure Ti alloy ingot melted prior to melting the constituent elements. For the homogeneity mixing of constituent elements, each ingot was re-melted at-least five times. The mass reduction of each ingot alloy during melting was less than 1% of the original mass as weighted by constituent elements before put in arc machine and after make master alloy ingot. Ribbon samples were prepared by re-melting the ingots in the melt spinning machine. Ingots were first smash into pieces by hammering it, 8-10 gram of ingot piece of each alloy was loaded in a fused quartz crucible which has a nozzle with diameter of 1~2 mm. After fixed crucible in the chamber, by making it evacuated and back filled under Argon gas, ingot piece inductively re-melted in a crucible and then injected with the pressure of 35 KPa through a nozzle onto a spinning copper wheel having speed 40 m/s, adjust by considering the ingot alloy

composition. Ribbon samples of different compositions were made, which have thickness of around 40 um and width of around 2 to 3 mm. The sixth ribbon sample, $Fe_{79.3}B_{16.4}Si_4C_{0.3}$, having thickness of around 40 μm, provided by Professor Eun Soo Park. A figure 2.1 shows the steps of making ribbon samples from individual elemental constituents.

For the structural characterization, x-ray diffraction (XRD) was used in order confirm the amorphous nature of metallic glass ribbon samples. Because of smaller thickness and width of ribbons, the layers of as synthesized ribbons were made on glass slide by placing free side of ribbon on each other in order to provide a larger target for x-rays. Diffraction spectra was acquired using a new D8 advance x-ray Diffractometer having continuous maximum output power of 3000W, with high voltage of 10 to 60 Kv with a collimated cobalt K_α x-ray source (λ=1.5405 Å). XRD pattern of ribbon samples were collected in 2θ, typically over 20-80^o. X-ray diffraction results for all metallic glasses are shown in figure 2.2. All the results show the broad range peak without any sharp crystalline peak give strong evidence that all the metallic glass ribbons have the amorphous nature.

2.2. Bending/ Bending fatigue test

A bending test was performed between two parallel platens. In which

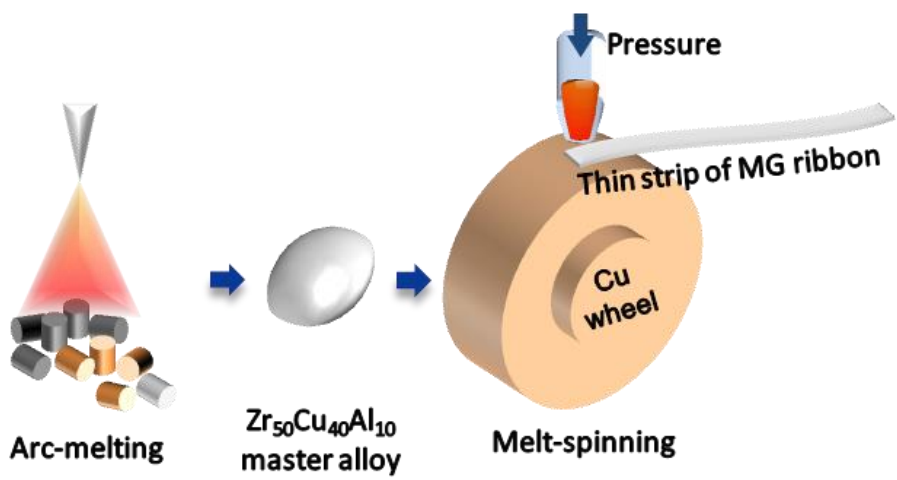

Figure 2.1. Fabrication process of making ribbon samples from individual elemental constituents.

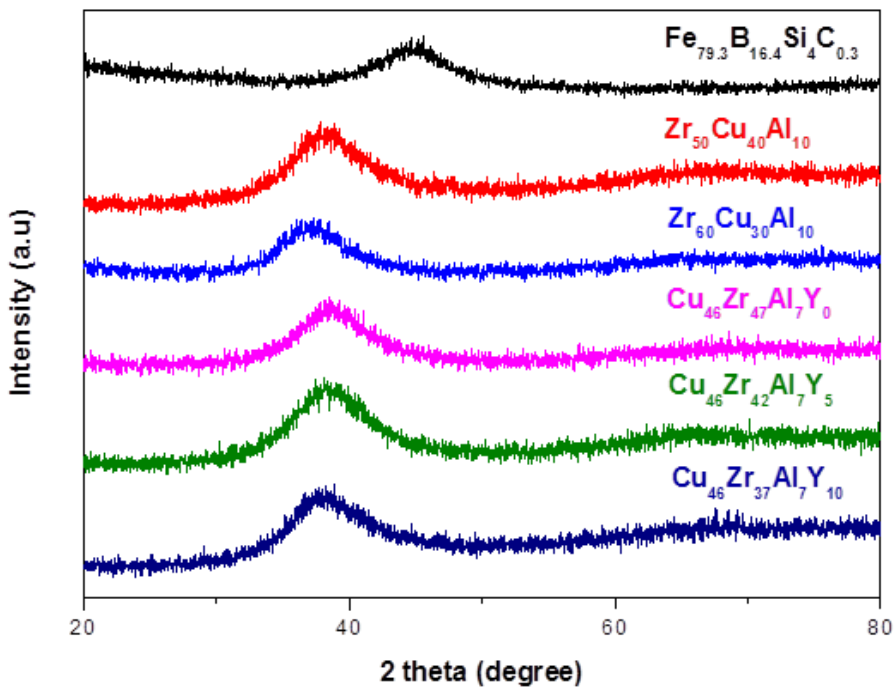

Figure 2.2. XRD diffraction pattern of monolithic $Fe_{79.3}B_{16.4}Si_4C_{0.3}$ $Zr_{50}Cu_{40}Al_{10}$, $Zr_{60}Cu_{30}Al_{10}$, $Zr_{47}Cu_{46}Al_7$, and non monolithic $Cu_{46}Zr_{42}Al_7Y_5$, $Cu_{46}Zr_{37}Al_7Y_{10}$ metallic glasses.

one plate is fixed while other plate is moving towards the fixed plate. The motion of the moving plate is driven by the servo-controlled electric motor. The moving plate can be moved at different speeds and it can be stopped at different distances from the fixed plate. The minimum distance between plates should be kept double of the thickness of the ribbon sample while the maximum distance depends on the length of ribbon using under considerations. The speed of the moving plate and distance between plates is controlled by software. The schematic of the bending plates shown in the figure 2.3 (a). For the optimum results, the ribbon sample should be small enough so that it cannot cross the upper surface of plates, while it should long enough so that it remains up from the screw holes, as shown in figure 2.3 (b). In figure 2.3 (b), the P represents the force that applied to ribbon by bending plates, D represents the distance between plates, while d represents the thickness of ribbon and r represents the curvature of ribbon. All metallic glass ribbons that used for bending test have length of around 30 mm. The ribbon sample of desired length was cut by scissor from a long strip of ribbon and then polish the sides of the ribbon by 2000 grit paper. After polishing the remaining width of ribbon is around 1.5 ~ 2 mm, and it fixed in screws of moving and fixed plates, as shown in the below figure 2.3 (a). The bending test is proceeded by moving the moving plate at a certain speed and stop at a certain distance. After finishing the experiment, the moving plate has to move back to original position and ribbon sample removed from the screws, this ribbon sample clearly shows the kinking (kink angle) at the center. The fixing of ribbon in screws is very important, because if the

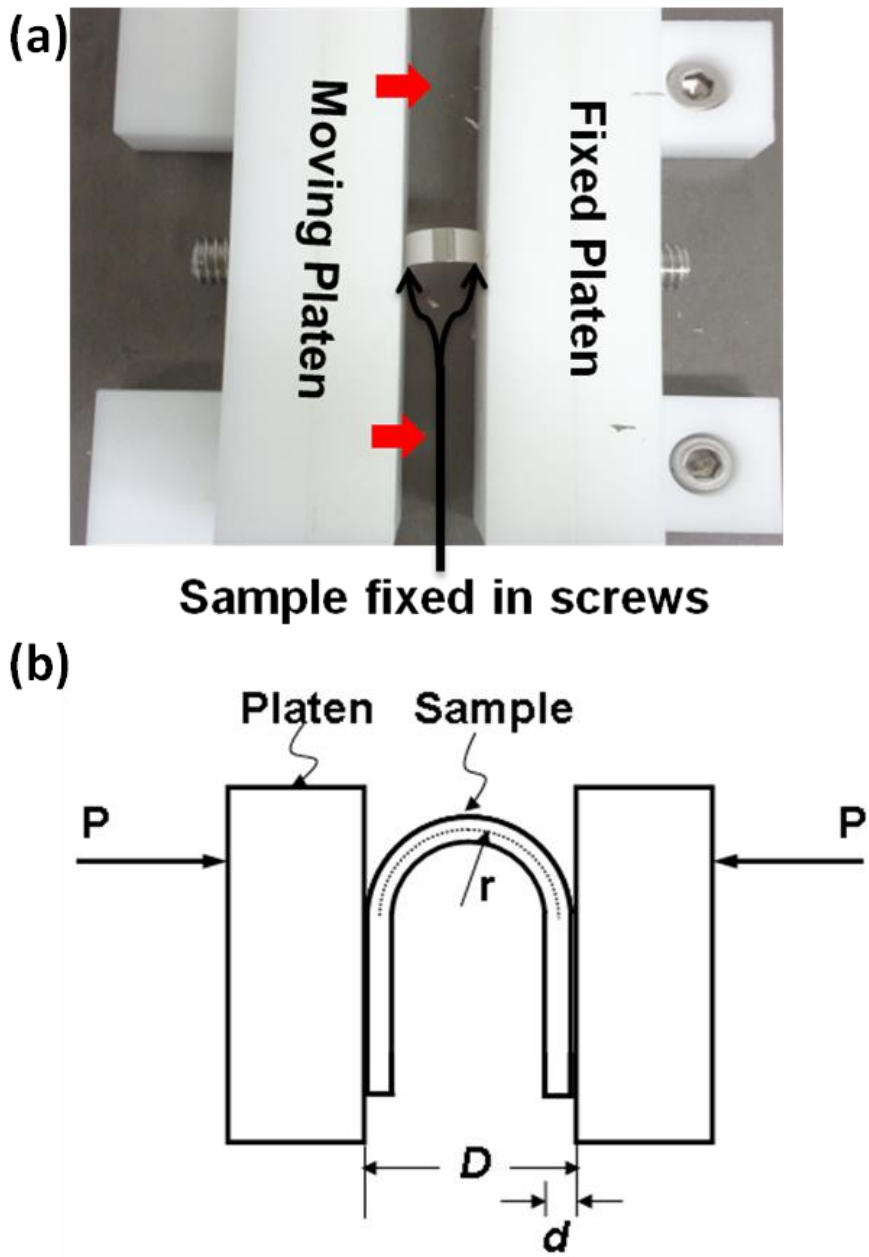

Figure 2.3. (a) The schematic of the bending plates. (b) The adjustment of ribbon between bending plates for the optimum results.

ribbon tilted from the semi-circle as shown in figure 2.3 (b) then the resulting kinking will be not accurate and it damage the desired mechanical properties of kinked ribbon sample. By applying different speeds to the moving plate and by adjust the different final distances between plates, different kinking happened as shown in the below figure 2.4. A kink angle value of ribbon samples after bending test were measured with the help of micro-scope at the magnification of 100x. An image of kinked ribbon samples were captured by microscope as shown in figure 2.5. After capturing the image, a rectangle was drawn which crossed the sides of ribbon. Two straight lines were drawn from the point of touching of ribbon sides and rectangle towards the center. The crossing of straight lines at center gives the kink angle value which measure by drawing arc as can see in figure 2.5. Below figure 2.5 clearly shows the difference of kink angle values depending on the kinked ribbon samples which get at different bending conditions, like as figure (a) has kink angle of 79.9^{o} at the speed of 0.64 mm/sec and at the final distance of 0.25 mm between plates for $Zr_{50}Cu_{40}Al_{10}$ metallic glass ribbon, while the same metallic glass ribbon shows kink angle of 35.5^{o} when the speed between plates is around 0.002 mm/sec and the distance is 1.1 mm as can seen in figure (b).

A bending fatigue test was performed in order to measure the fatigue limit of alloy system. A fatigue test was performed between two platens whose perpendicular distance (d) adjusts according to required strain. The plates slides parallel to each other with sliding distance of 10 mm at reciprocating frequency of 1 Hz. The schematic of bending fatigue plates

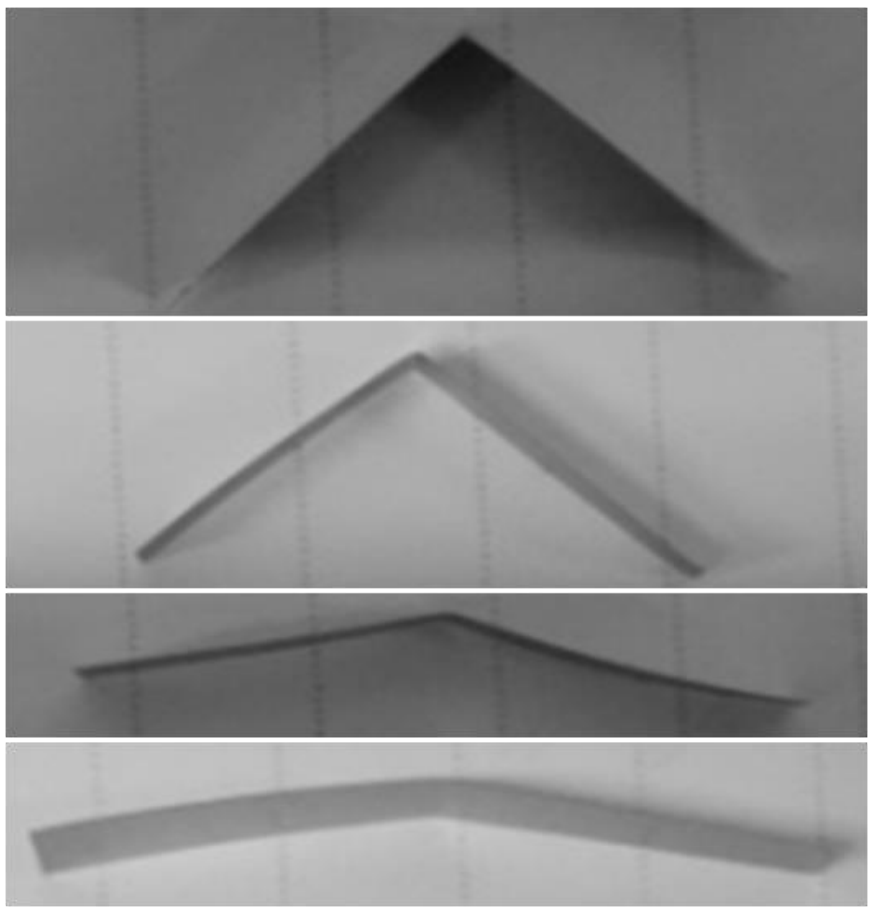

Figure 2.4. Kinking of ribbon samples at different speeds of moving plate and different final distances between plates.

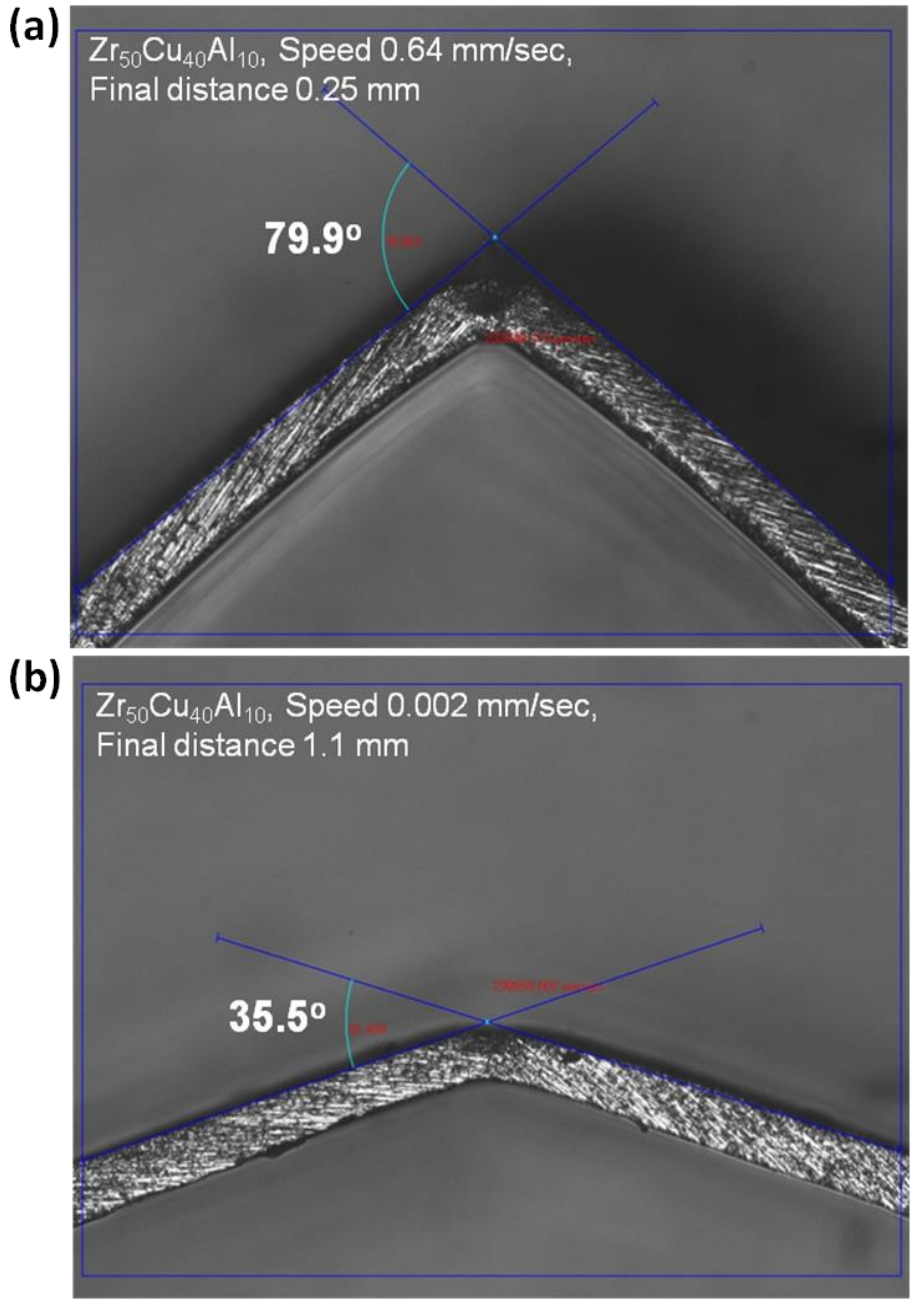

Figure 2.5. Kink angle value after bending test which measured by microscope. Figure (a) shows the kink angle of 79.9° while figure (b) shows kink angle of 35.5°.

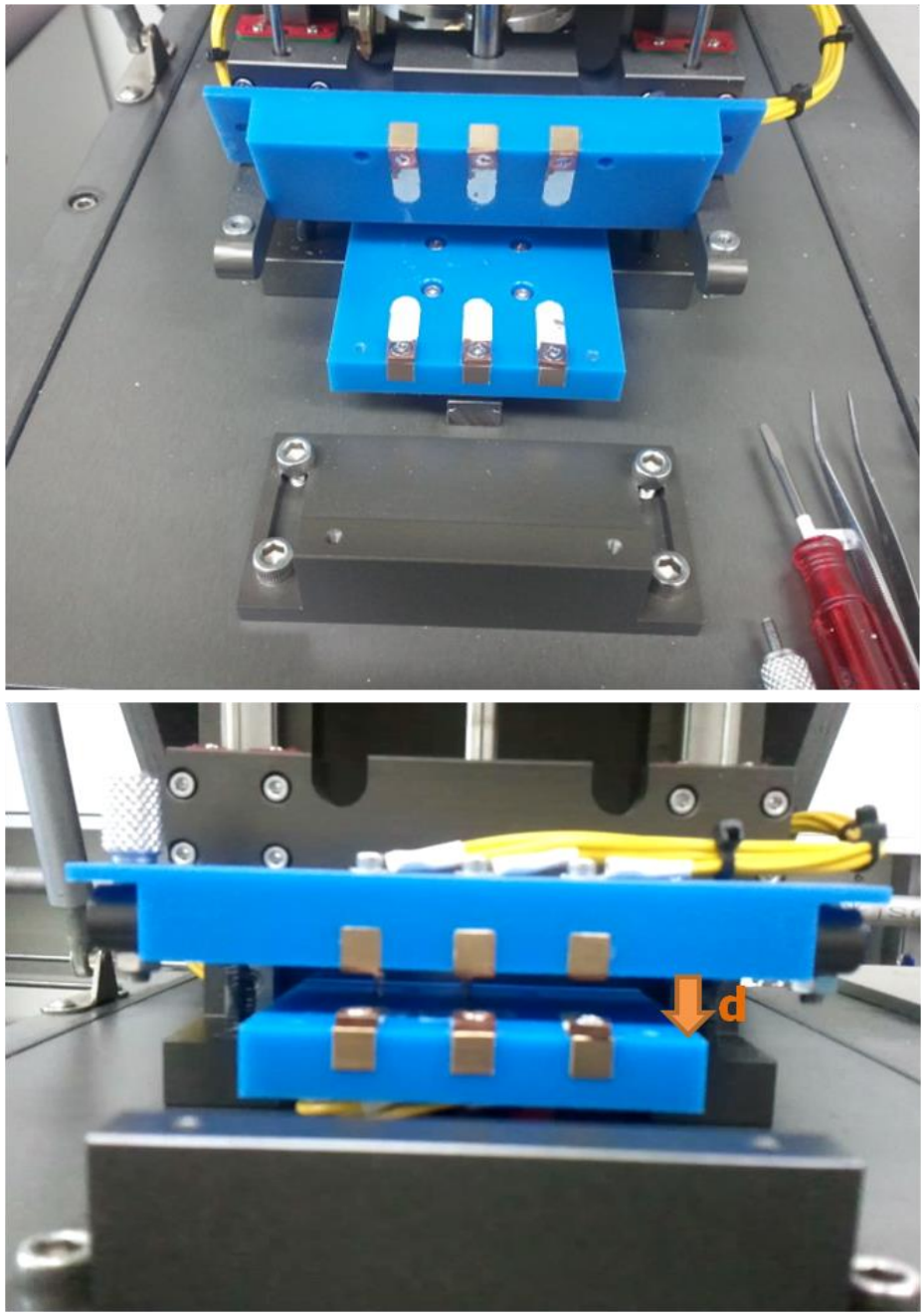

Figure 2.6. Bending fatigue test machine.

shown in figure 2.6. At different strains, the life time (number of cycles) were varied for different alloys. By using Basquin's law (high cycle fatigue), the fatigue strength of system can be easily calculated [28-29]. Basquin's law;

$$\sigma_a = \frac{\Delta\sigma}{2} = \frac{\Delta\epsilon_e E}{2}$$

Where σ_a is fatigue strength at specific strain, ε_e is strain and E is elastic modulus.

2.3. Static observation of shear bands

Deformed region (kinked region) of metallic glass ribbon samples after bending test at specified conditions were observed with the help of JSM-6360 scanning electron microscope having W filament as a electron source and SE resolution of 3 nm (at 30KV) (RIAM, SNU). After bending test, samples were cleaned with acetone by using ultrasonic cleaner for at-least three minutes. After cleaning ribbon samples, it suddenly dried with high pressure air so that acetone droplets completely removed from ribbons because of its high cooling rate. After dried, ribbon samples were pasted with carbon black tape on the holder which has height stages, which makes the observation of deformed region at the center of the ribbon by making it horizontal instead of cutting of ribbon sample at the center.

2.4. Dynamic observation of shear bands

For the shear band kinetics (shear band density with time) of brittle ($Fe_{79.3}B_{16.4}Si_4C_{0.3}$) and ductile ($Zr_{50}Cu_{40}Al_{10}$) metallic glass ribbons, a direct observation of shear bands was done during the bending test. A micro-scope was fixed on the top of the bending machine which can be move in all directions by considering the focusing of ribbon sample under bending test, as can see in the figure 2.7. Shear band can be easily observed through the micro-scope by naked eye during bending test, while in order to observe live image of shear band during bending test from micro-scope to computer, a camera was used on the top side of microscope which can capture 25 frames per second. In this case we can easily focus the images capturing by moving the micro-scope up and down, while it can be move towards right as the bending test proceed during the motion of the moving plate. In order to more clearly observed shear bands a glass slide pasted with carbon black tape at the top surface of bending plates so that the ribbon shows same exterior to micro-scope during bending test and the focusing of micro-scope remain same during bending test. Also it noticed that a normal tube light is not enough to see the nucleation of shear band, in order to solve this problem an extra high light intensity source was used which can be adjust according to position of ribbon sample and at maximum focusing for the observation of shear band.

Figure 2.7. Bending machine for the shear band kinetics.

2.5. Nano-indentation

A nano-indentation test was conducted in order to observe the structural heterogeneity of brittle and ductile metallic glass ribbon samples. A conical tip of indenter was used for all of ribbon samples. A ribbon sample (having thickness of around 40 μm) mounted with the round clip holder. After mounted become harden, both sides of mount make smooth by polisher in room temperature. Different grit papers (600 to 4000) were used to polish surface at both sides of mount and finally, surface makes refined by using 0.01 NaCl liquid and white grit paper. Multiple indents were carried out on each ribbon with sides towards indenter. Nano-indentation experiment have the specification of; loading rate of 0.25 mN/s in a constant state with the loading control mode and the maximum force applied is around of 10 mN which unloaded with the rate of 1 mN/s in a constant state by holding it for around 30 seconds.

2.6. Micro-Indentation

Micro hardness test was performed with a help of Durascan 70 indenter machine. An indenter with a pyramidal shape was applied to different metallic glass ribbon samples at different loads. The ribbon samples (having width around 2 to 3 mm and length around 10 mm) with air side up were pasted on the aluminum block by using carbon black tape. A 100 and 200 gram loads were used for measuring the hardness of ribbon samples. At-least fifty indents

were applied to each metallic glass ribbon with 36 seconds of interval between each indentation and the data for hardness was used by choosing appropriate points among the all indented points. The hardness value was automatically calculated by software. Shear band morphology (scale pile-up shear bands) was observed by scanning electron microscope (SEM). Number of scale pile-up shear bands altered for different metallic glass ribbon samples at the same load.

Chapter 3. Results and Discussion

3.1. Correlation between kink angle and shear band evolution under bending test

By applying specific bending conditions (distance between plates and speed of moving plate) the kink angle of metallic glass ribbon samples were calculated as explained in section 2.2. An estimated strain rate $|\dot{\epsilon}|$ was calculated by taking the differential of $\epsilon = \frac{d}{D-d}$ [30].

$$|\dot{\epsilon}| = |\frac{d}{dt}\left(\frac{d}{D-d}\right)| = \frac{Sd}{(D-d)^2}$$

Where D is separation distance between platens which I use from 0.25 mm to 1.1 mm between plates, while d is thickness of ribbon sample which is around 40 μm and S is platen speed which I use from 0.001 mm/sec to 1.28 mm/sec of moving plate. A relationship between kink angle and estimated strain rate for $Zr_{50}Cu_{40}Al_{10}$ alloy metallic glass ribbon samples under various experimental conditions was calculated, as shown in figure 3.1. It noticed that at the higher speed (higher estimated strain rate), the kink angle value is lower as compared to at lower speed (lower estimated strain rate) when the distance between plates is lower. The kink angle going to increase as the strain rate is getting lower under the same lower bending distance between plates. While it observed that the kink angle approaches same value at different strain rates at the lower distance between plates. Deformed

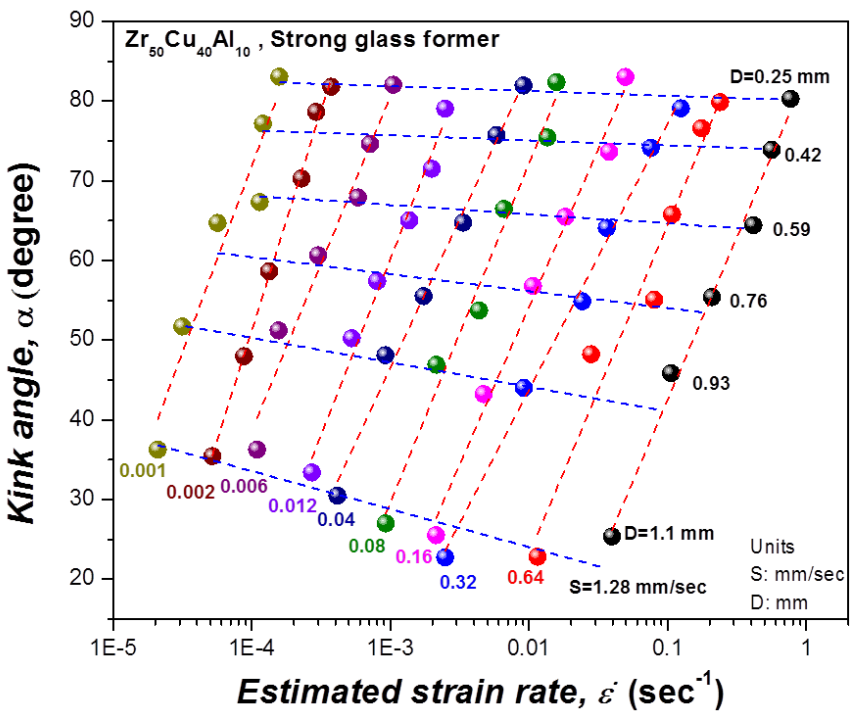

Figure 3.1. Relationship between kink angle and estimated strain rate for $Zr_{50}Cu_{40}Al_{10}$ metallic glass ribbon samples at various speeds of moving plate and at different distances between plates.

region of ribbon samples at different estimated strain rates which have different kink angle were observed under scanning electronic microscope (SEM). The SEM images at lower and higher estimated strain rates with respect to lowest and highest distance between plates that used in this research are shown in figure 3.2 and 3.3 respectively. It can be seen from figure 3.2 that at higher estimated strain rate (points d, e and f) only fewer shear band generated. While at lower estimated strain rate (points a, b and c) multiple shear bands generated. The higher shear band density (number of shear bands/ region) at lower estimated strain rate, causes higher kink angle as compared to higher estimated strain which has fewer shear bands. Because of larger shear band density at center, the recovering curvature of ribbon after removal of bending forces is less and it basis of higher kink angle at lower estimated strain rate. At higher strain rate, the forces effect on the atoms is less and less sliding of atoms happened which cause fewer shear bands generation due to less free volume creation in metallic glass. While at lower strain rate, the forces effect is higher on the atoms because of low speed and it causes multiple shear bands generation due to high free volume generation in metallic glass because of higher movement of atoms across each other. By considering figure 3.3, we can see that the shear band density is almost similar at different strain rates and that's the reason that at lower distance between plates the kink angle approaches same value for all estimated strain rates. The shear band density at the center causes almost similar recovering curvature at all strain rates which give the similar kink angle at lower distance between plates.

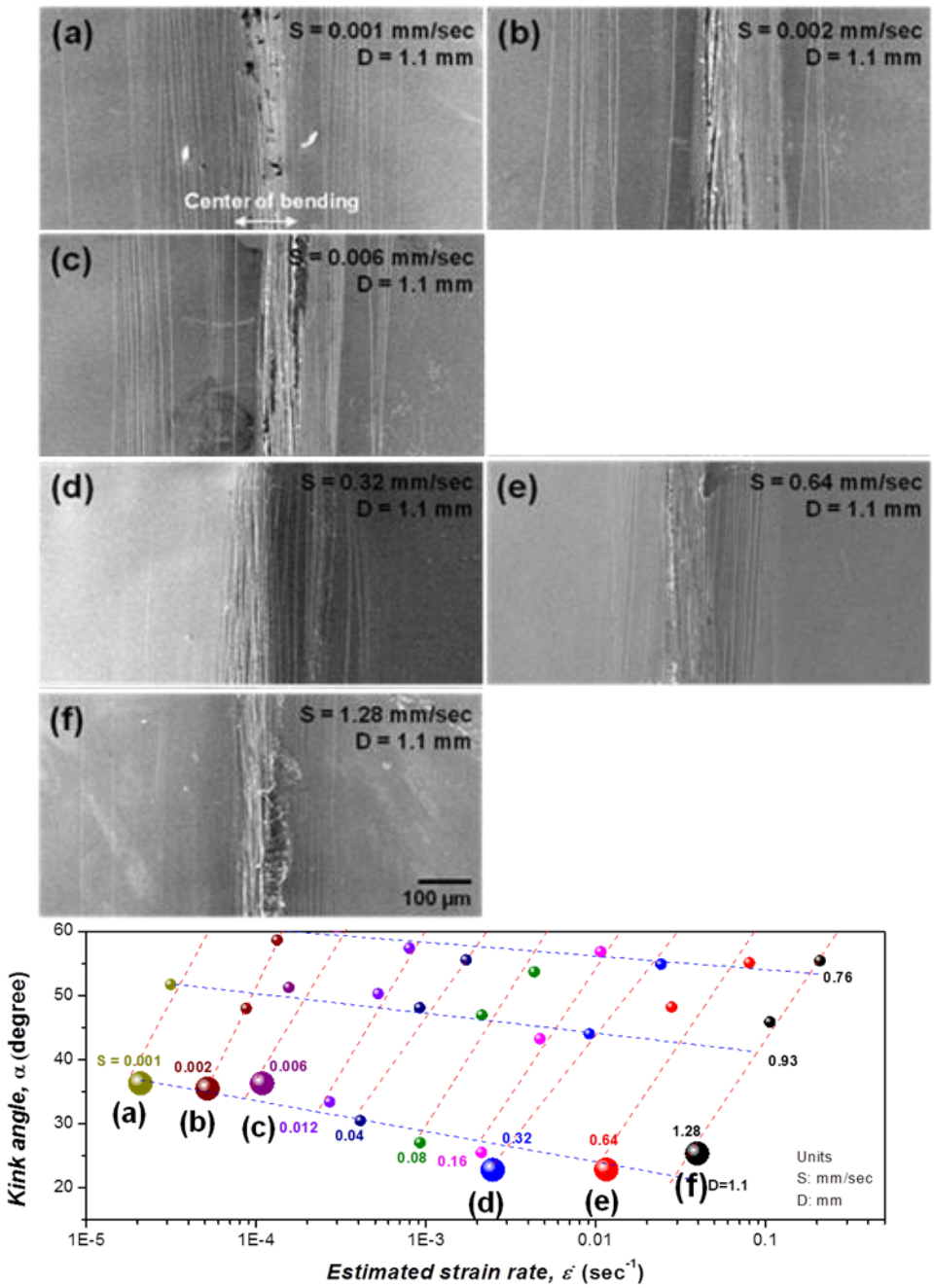

Figure 3.2. The deformed region observation under SEM for $Zr_{50}Cu_{40}Al_{10}$ metallic glass ribbons at higher and lower estimated strain rates for 1.1 mm distance between plates.

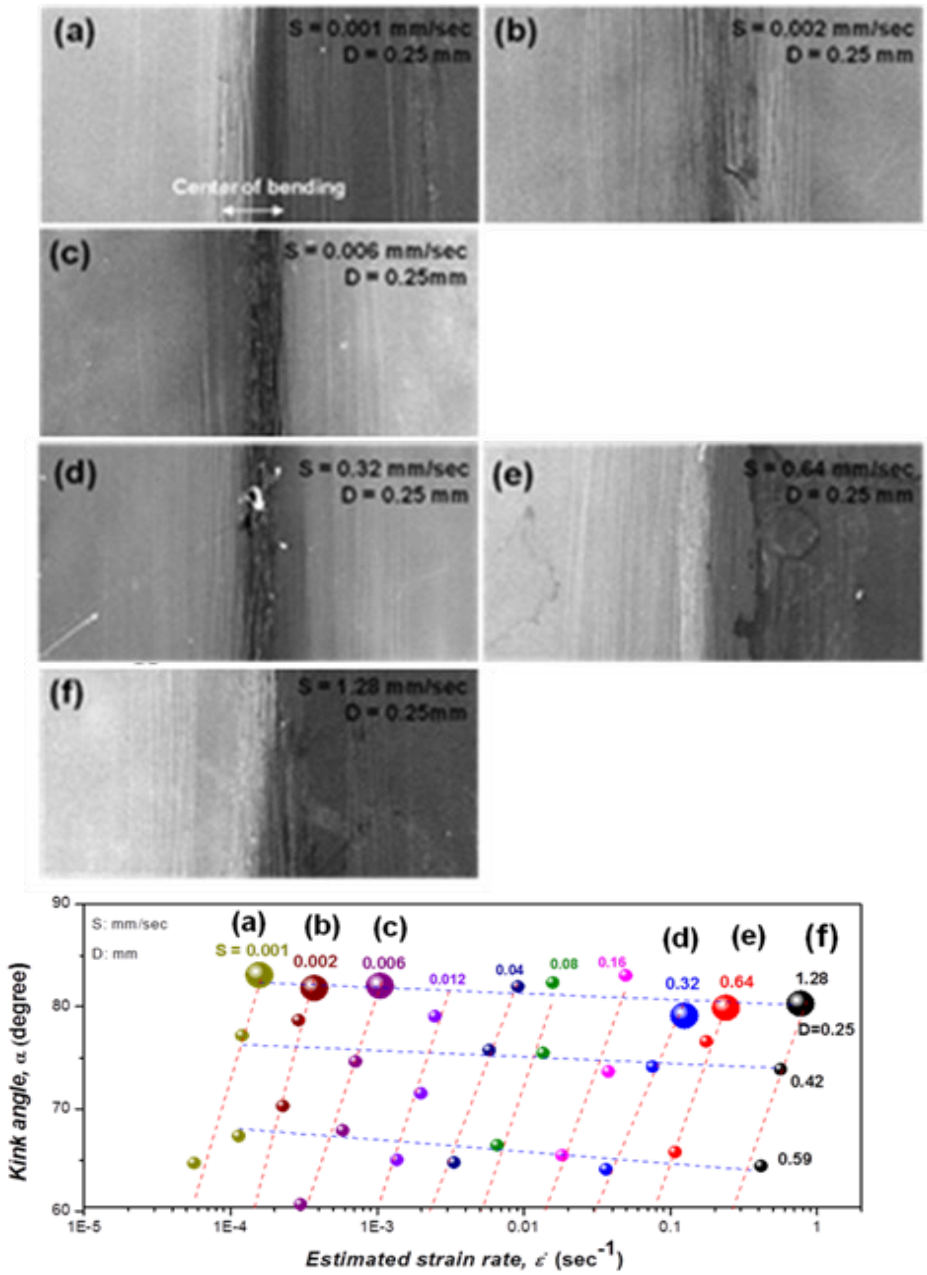

Figure 3.3. The deformed region observation under SEM for $Zr_{50}Cu_{40}Al_{10}$ metallic glass ribbons at higher and lower estimated strain rates for 0.25 mm distance between plates.

By considering the corner points of kink angle versus estimated strain rate relation, as can see in figure 3.4 and 3.5, a dependence of shear band morphology on kink angle variation can more clearly noticeable. As can see in figure 3.4, at lower distance (0.25 mm) between plates (points a and b) the shear band density is higher as compared to higher distance (1.1 mm) between plates (points c and d). The enlarge area of shear band region of figure 3.4, as shown in figure 3.5 clearly mentioned the shear band density difference depends on kink angle variation. At the distance of 0.25 mm between plates (points a and b), the shear band density is around 16 at the speed of 1.28 mm/sec, which gives the kink angle around 80.277^{o} (point a), and at the kink angle of 83.065^{o} when the speed between plates is 0.001 mm/sec the shear band density is around 19 (point b). Similarly by comparing the shear band density at higher distance (1.1 mm) between plates (points c and d), it noticed that the shear band density is around 7 when the speed of moving plate is 1.28 mm/sec and it gives kink angle around 25.350^{o} (point c), while at the speed of 0.001 mm/sec when kink angle is around 36.368^{o} the shear band density is 10 (point d).

By magnifying the deformed region of ribbon after bending test, we can more clearly observe the difference of shear band morphology at center middle and edge part of deformed ribbon, as can see deformed region in figure 3.6 for fragile metallic glass ($Zr_{60}Cu_{30}Al_{10}$) ribbon after bending test at distance of 1.1 mm between plates with speed of 0.001 mm/sec which gives kink angle of around 35.286^{o}. The center region of
ribbon is more deformed as compared to middle and edge region. The

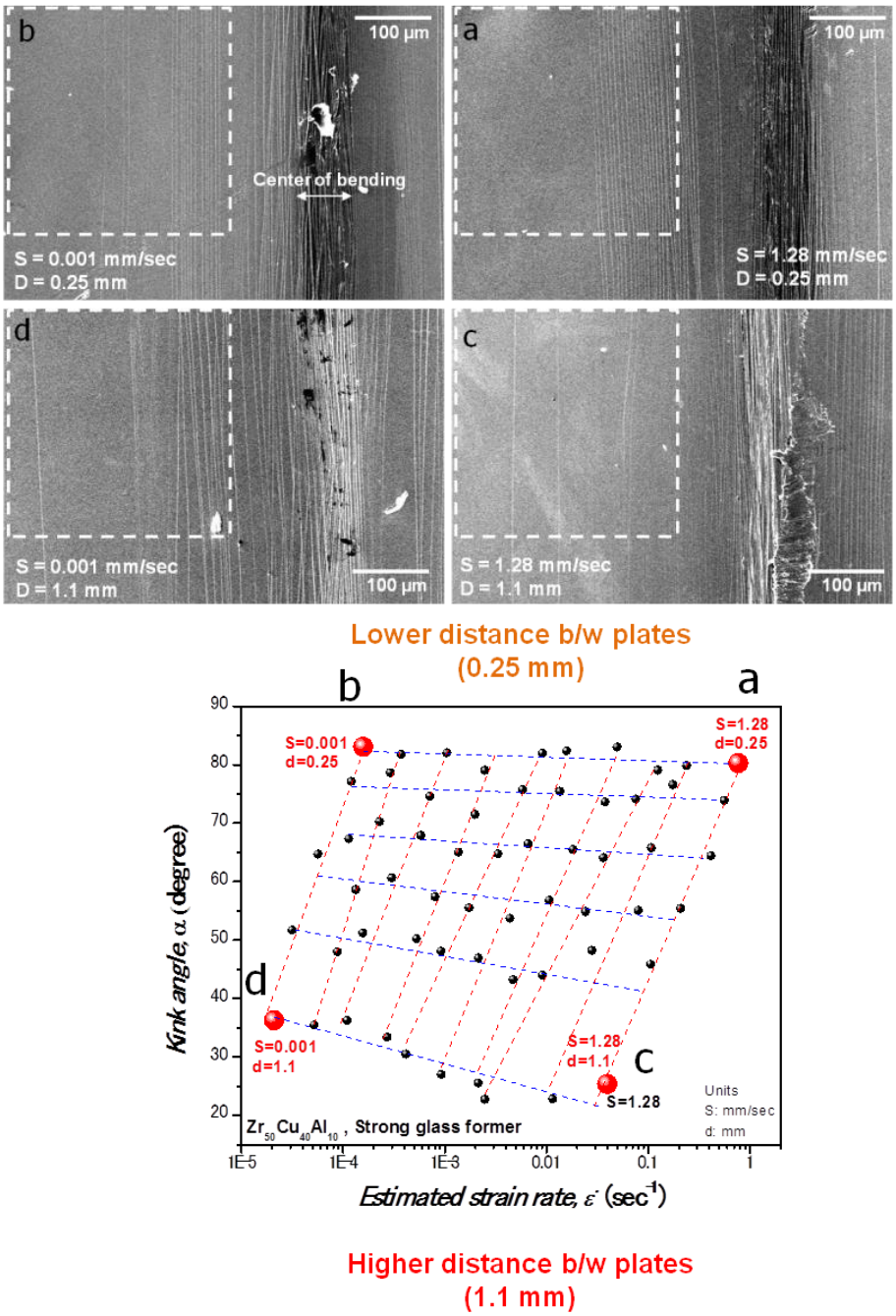

Figure 3.4. The deformed region observation under SEM for $Zr_{50}Cu_{40}Al_{10}$ metallic glass ribbons at corner points of kink angle versus estimated strain rate relation.

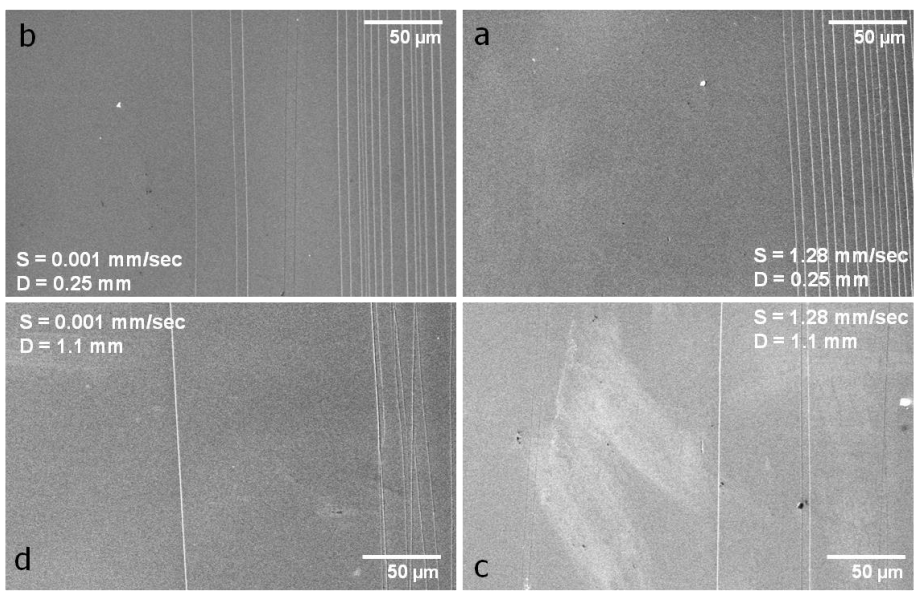

Figure 3.5. The enlarge area of shear band region of figure 3.4 which represented by dashed rectangles.

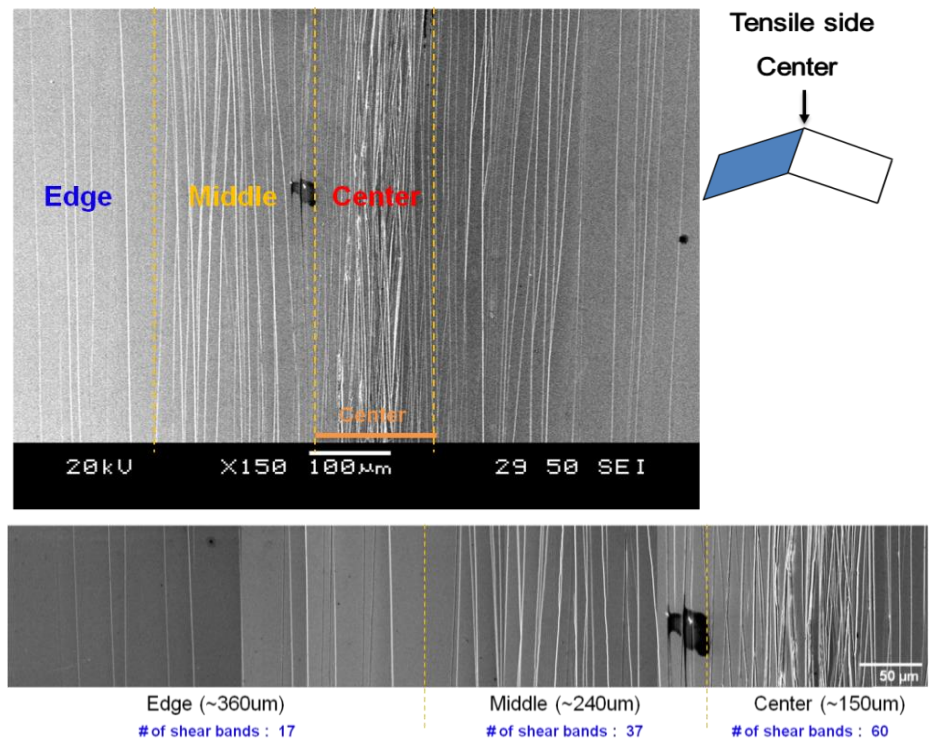

Figure 3.6. Deformed region of fragile metallic glass ($Zr_{60}Cu_{30}Al_{10}$) ribbon with magnified center, middle and edge part, after bending test at distance of 1.1 mm between plates with speed of 0.001 mm/sec.

center region has concentrated rough shear band area with shear band density around 60, while the middle region has mostly closed crossing shear bands with shear band density around 37 and the edge part has mostly spaced single shear bands with shear band density around 17. The total deformed region is around 750 μm, which consist of center (around 150 μm), middle (around 240 μm) and edge (around 360 μm).

By extrapolating the relation between kink angle and estimated strain rate to kink angle initiation (kink angle = 0), gives the approximate value of shear band initiation or yield point of metallic glass as shown in below figure 3.7. In this case the shear band initiation at speed of 1.28 mm/sec happened approximately at strain rate of 9.039×10^{-3} (sec^{-1}), which gives yield point around 2.41 mm of distance between plates while the speed of 0.001 mm/sec gives the yield point around 3.76 mm at the strain rate of 2.89×10^{-6} (sec^{-1}) for the kink angle initiation.

3.2. Comparison between brittle and ductile metallic glasses depending on alloy system

The brittle metallic glasses have normally higher strength as compared to ductile metallic glasses. A comparison table 3.1 [31, 32] of brittle (Fe based alloy) and ductile (Zr based alloy) metallic glasses are shown below. It shows that brittle metallic glasses have higher young modulus, yield strength and hardness as compared to ductile metallic glasses. The major

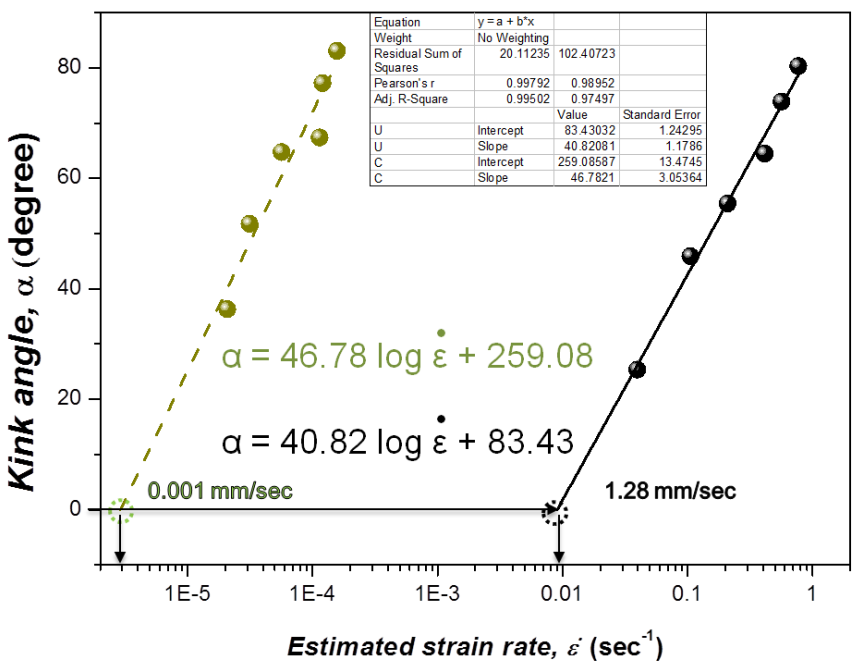

Figure 3.7. Approximation of yield point by extrapolating the relation between kink angle and estimated strain rate to kink angle initiation point (kink angle = 0) at speed of 1.28 mm/sec and 0.001 mm/sec.

problem with brittle metallic glasses is their zero plasticity nature. As can see in figure 3.8, the Fe based metallic glass shows very high strength but it shows zero plasticity, as can observe through mirror like fracture surface which is one of characteristic of brittle metallic glasses. While as compared to brittle metallic glasses, the ductile metallic glasses clearly shows plasticity, as can see in figure 3.9, the Zr based metallic glass shows lower strength but it has higher plasticity, as can also notice through the vein pattern on the fracture surface which is one of the characteristics of ductile metallic glasses [33, 34].

3.2.1. Shear bands evolution under bending test depending on kink angle variation

The relation between kink angle and estimated strain rate for brittle ($Fe_{79.3}B_{16.4}Si_4C_{0.3}$) and ductile ($Zr_{50}Cu_{40}Al_{10}$) metallic glasses were also calculated as shown in figure 3.10. It shows that the brittle metallic glass has higher kink angle as compared to ductile metallic glass at the same estimated strain rate. Because of higher yield strength of $Fe_{79.3}B_{16.4}Si_4C_{0.3}$ metallic glass as compared to $Zr_{50}Cu_{40}Al_{10}$ metallic glass, the shear band initiation happened at smaller distance between plates while in case of $Zr_{50}Cu_{40}Al_{10}$ metallic glass the shear band generated at early stage. As the shear band generated at smaller distance between plates for Fe based ribbon sample, it has smaller deformation region under bending forces and it causes

Alloy	Young Modulus	Yield Strength	Hardness
Fe based ribbon	165 GPa	3.212 GPa	13 GPa
Zr based ribbon	80 GPa	1.812 GPa	5 GPa

Table 3.1. Physical properties of brittle (Fe based alloy) and ductile (Zr based alloy) metallic glasses [31, 32].

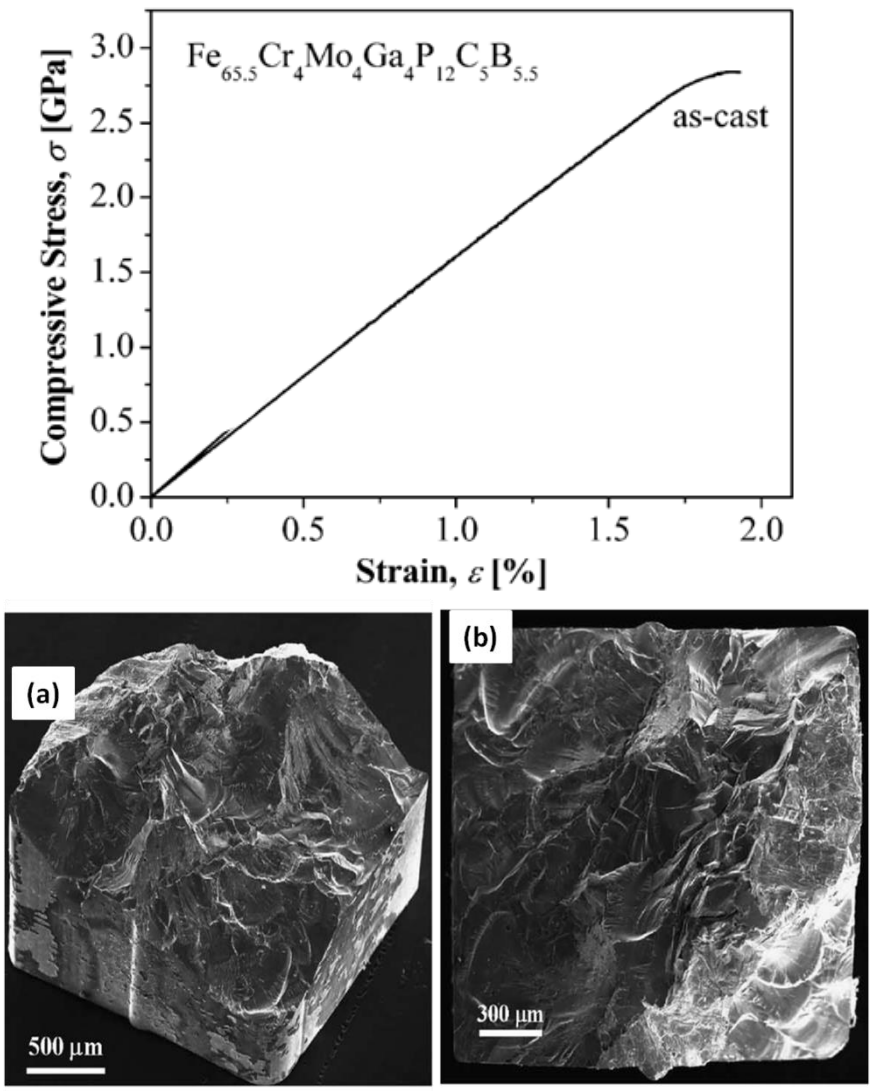

Figure 3.8. Stress-strain curve and fracture surface of brittle (Fe based alloy) metallic glass with magnified surface (b) from (a) [33].

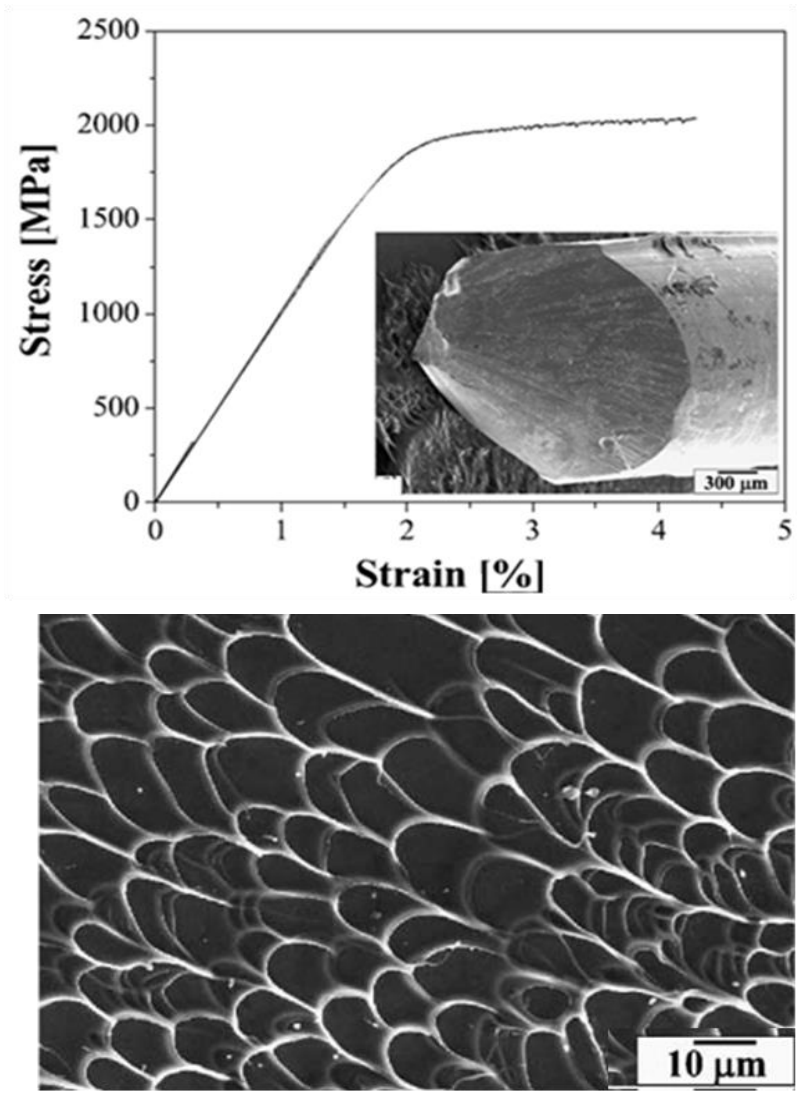

Figure 3.9. Stress-strain curve and fracture surface of ductile (Zr based alloy) metallic glass [34].

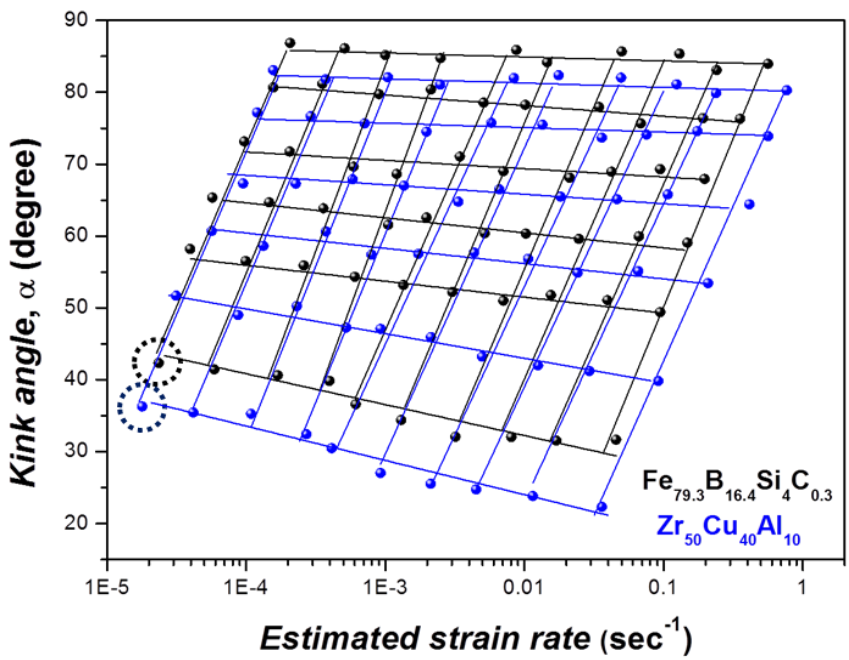

Figure 3.10. Relation between kink angle and estimated strain rate for brittle ($Fe_{79.3}B_{16.4}Si_4C_{0.3}$) and ductile ($Zr_{50}Cu_{40}Al_{10}$) metallic glasses.

the concentrated shear band at small region. While in case of initiation of shear band at larger distance between plates, $Zr_{50}Cu_{40}Al_{10}$ metallic glass has larger deformed region with widely spaced shear band. The shear band morphology difference for brittle and ductile metallic glasses can be easily observed under SEM, as shown in below figure 3.11 for Fe and Zr based ribbon samples, which measured at distance of 1.1 mm between plates with speed of 0.001 mm/sec of moving plate and it gives kink angle of 42.344^o for $Fe_{79.3}B_{16.4}Si_4C_{0.3}$ and 36.277^o for $Zr_{50}Cu_{40}Al_{10}$ metallic glasses. The (a) side of figure 3.11 shows the schematic diagram and SEM image of Fe based ribbon sample while the (b) side of figure shows the Zr based ribbon sample. From the SEM images we can clearly noticed that Fe based ribbon sample has concentrated shear band with the deformation region of only 400 μm, while Zr based ribbon sample has widely spaced shear band with large shear band region of 700 μm. Because of concentrated shear band at center, the center region is deformed much (characteristic of brittle metallic glasses) and this cause the less recovering of Fe based ribbon after removal of bending forces. While because of widely spaced shear band and less concentrated shear band at center which cause less deformation at center (characteristic of ductile metallic glasses), the recovering curvature for Zr based ribbon sample after removal of bending forces is higher and this cause the lower kink angle as compared to Fe based ribbon sample.

The step height of shear bands were also observed under optical surface pro-filometer for the brittle ($Fe_{79.3}B_{16.4}Si_4C_{0.3}$) and ductile ($Zr_{50}Cu_{40}Al_{10}$) metallic glass ribbons. The concentrated shear bands at

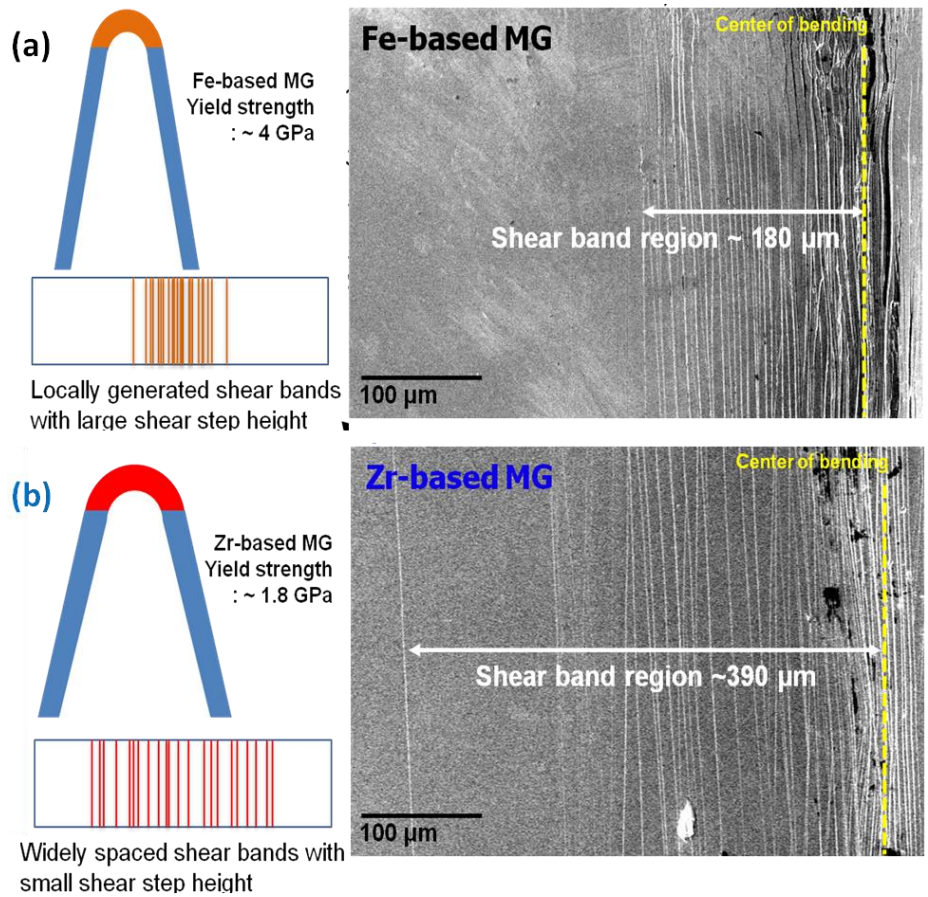

Figure 3.11 Schematic diagram and SEM image of $Fe_{79.3}B_{16.4}Si_4C_{0.3}$ (a) and $Zr_{50}Cu_{40}Al_{10}$ (b) metallic glasses, which measured at distance of 1.1 mm between plates with speed of 0.001 mm/sec of moving plate and it gives kink angle of 42.344º for $Fe_{79.3}B_{16.4}Si_4C_{0.3}$ (black circle at figure 3.7) and 36.277º for $Zr_{50}Cu_{40}Al_{10}$ (blue circle at figure 3.7) metallic glasses.

center for brittle ($Fe_{79.3}B_{16.4}Si_4C_{0.3}$) metallic glass causes higher step height as compared to ductile metallic glass which has less concentrated shear band at center. It was observed that the average shear step height for $Fe_{79.3}B_{16.4}Si_4C_{0.3}$ metallic glass ribbon is around 54.5 nm, while for $Zr_{50}Cu_{40}Al_{10}$ metallic glass ribbon is around 32.8 nm. The results of optical surface profile meter for brittle ($Fe_{79.3}B_{16.4}Si_4C_{0.3}$) and ductile ($Zr_{50}Cu_{40}Al_{10}$) metallic glass ribbons are shown in figure 3.12.

Shear band nucleation observation during bending test for brittle ($Fe_{79.3}B_{16.4}Si_4C_{0.3}$) and ductile ($Zr_{50}Cu_{40}Al_{10}$) metallic glass ribbons were done with the help of micro-scope as explained in section 2.4. The below figure 3.13 shows different distance stages of shear band captured images during bending test. While figure 3.14 (a) explained the relation between shear band density versus distance between plates and figure 3.14 (b) explained the relation between shear band density versus time for $Fe_{79.3}B_{16.4}Si_4C_{0.3}$ and $Zr_{50}Cu_{40}Al_{10}$ metallic glass ribbons. From figure 3.13 we can easily observe that as the bending test proceeding the shear band density is increasing. Observation of shear band during bending test (at speed of 0.016 mm/sec) shows that shear band initiated at early stage (larger distance between plates) in $Zr_{50}Cu_{40}Al_{10}$ ribbon as compared to $Fe_{79.3}B_{16.4}Si_4C_{0.3}$ ribbon as can see in figure 3.14 (a). It also shows that the shear band density with the distance between plates is higher for $Zr_{50}Cu_{40}Al_{10}$ metallic glass ribbon as compared to $Fe_{79.3}B_{16.4}Si_4C_{0.3}$ metallic glass ribbon. The initiation of shear band with the time is almost similar for both brittle and ductile metallic glasses at initial stage but in case of

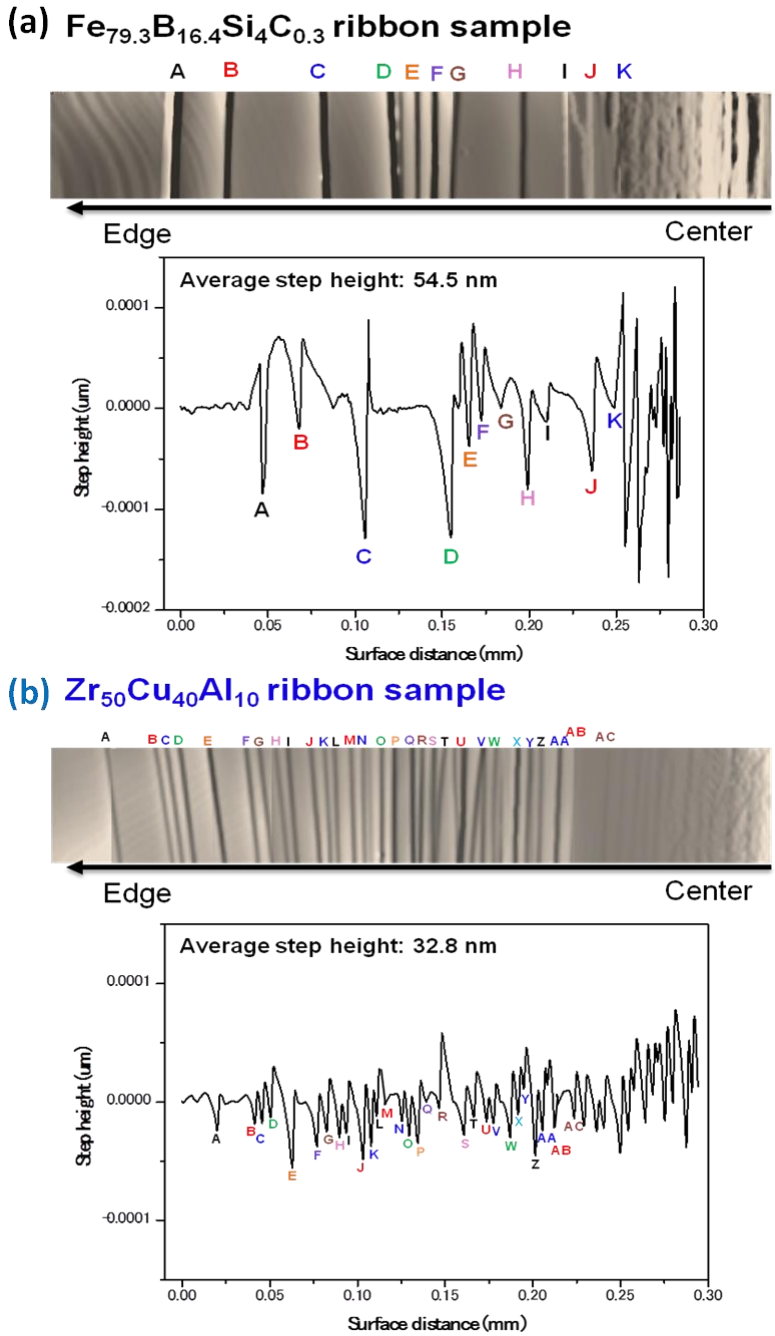

Figure 3.12. Step height observation of shear bands for brittle $Fe_{79.3}B_{16.4}Si_4C_{0.3}$ (a) and ductile $Zr_{50}Cu_{40}Al_{10}$ (b) metallic glasses.

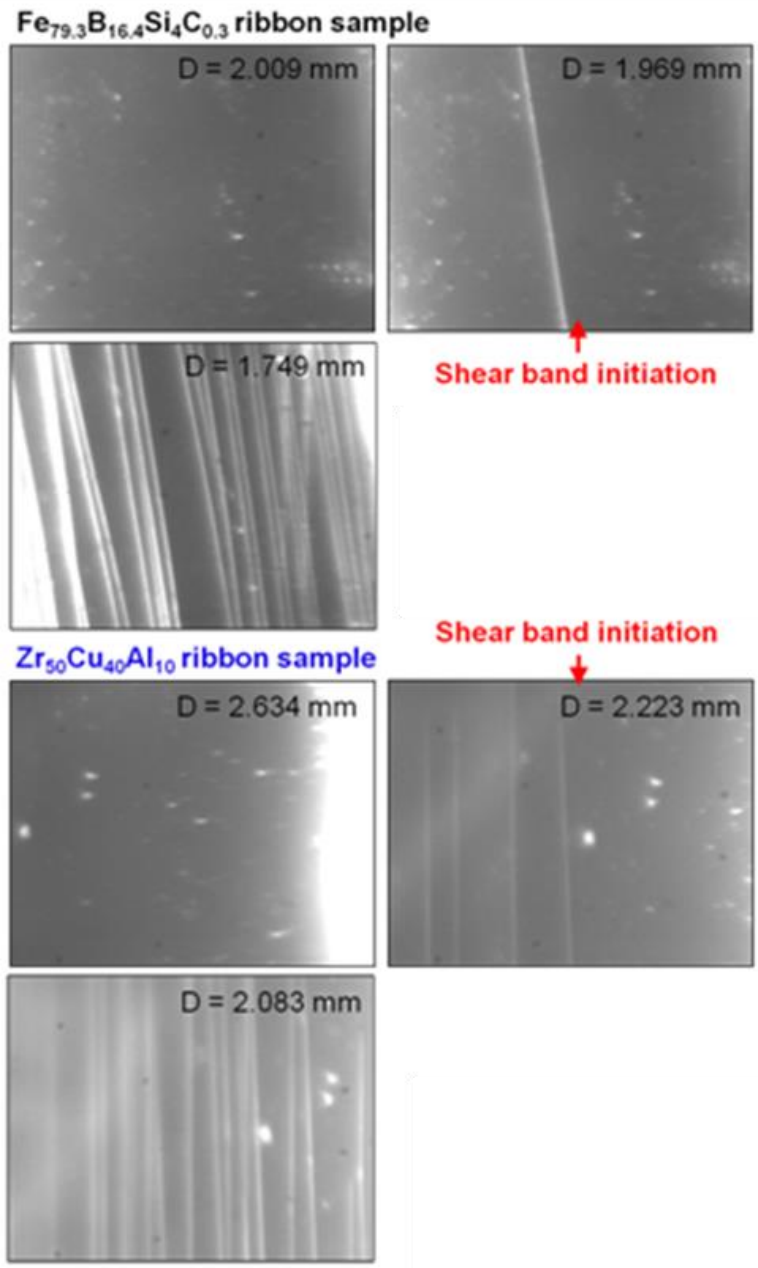

Figure 3.13. Captured image at different distance stages of nucleated shear bands for $Fe_{79.3}B_{16.4}Si_4C_{0.3}$ and $Zr_{50}Cu_{40}Al_{10}$ metallic glass ribbons during bending test.

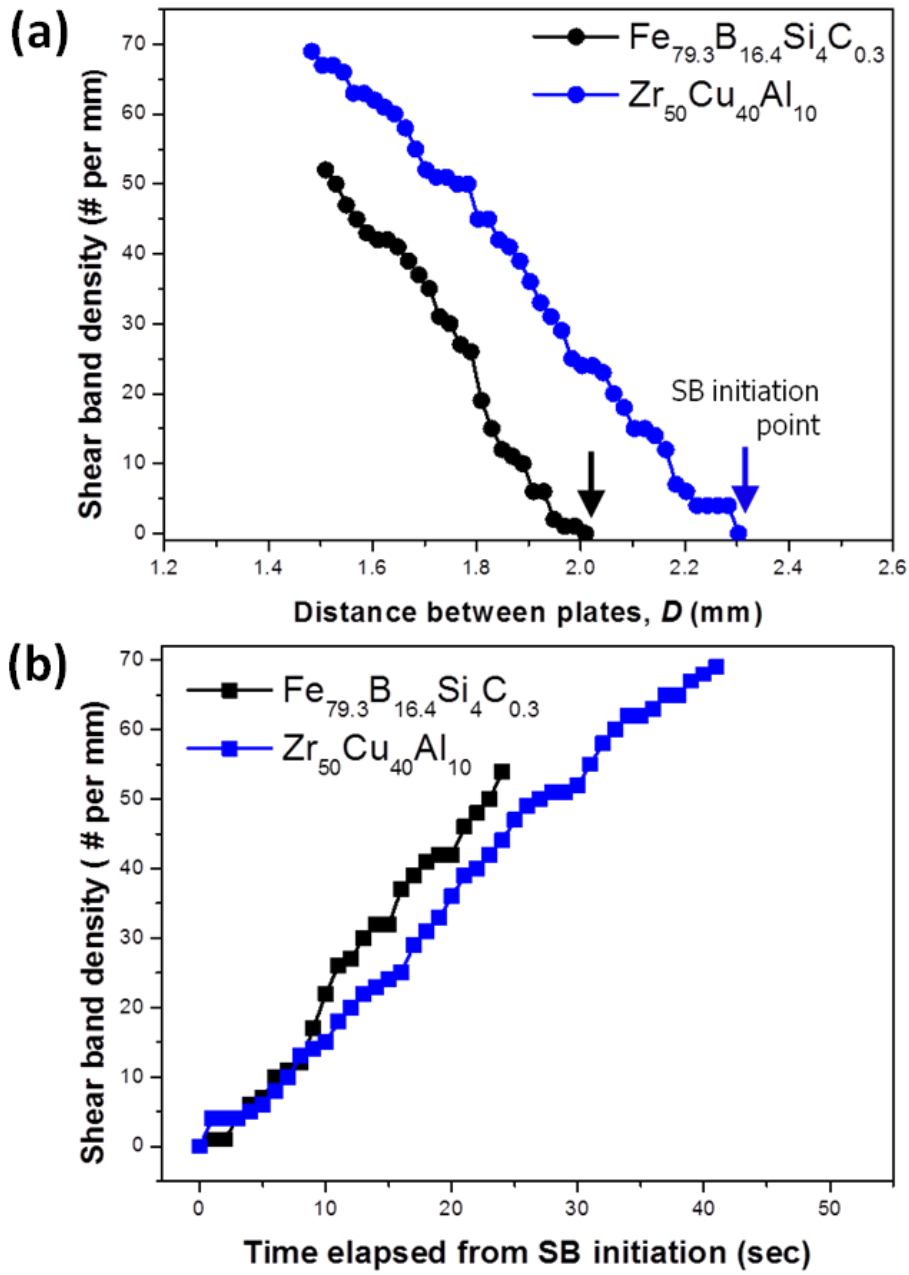

Figure 3.14. Relation between (a) shear band density versus distance between plates and (b) shear band density versus time of $Fe_{79.3}B_{16.4}Si_4C_{0.3}$ and $Zr_{50}Cu_{40}Al_{10}$ metallic glass ribbons during bending test.

$Fe_{79.3}B_{16.4}Si_4C_{0.3}$ ribbon the multiple shear band generated at short time while the nucleation of shear band with time for $Zr_{50}Cu_{40}Al_{10}$ ribbon is almost linear as can see in figure 3.14 (b). Because of the smaller deformation region and multiple generation of shear band at small region in short time, causes the higher kink angle of $Fe_{79.3}B_{16.4}Si_4C_{0.3}$ ribbon as compared to $Zr_{50}Cu_{40}Al_{10}$ ribbon.

The shear band initiation point was also determined through kink angle versus estimated strain rate relation at the speed of 0.012 mm/sec. By extrapolating the relation between kink angle and estimated strain rate to kink angle initiation (kink angle = 0), for $Fe_{79.3}B_{16.4}Si_4C_{0.3}$ ribbon and $Zr_{50}Cu_{40}Al_{10}$ ribbon gives the approximate value of shear band initiation as shown in below figure 3.15. In this case the shear band initiation at speed of 0.012 mm/sec happened approximately at strain rate of 6.77×10^{-5} (sec^{-1}), which gives shear band initiation point around 2.70 mm for $Fe_{79.3}B_{16.4}Si_4C_{0.3}$ metallic glass ribbon while at the same speed the shear band initiation point is around 2.91 mm at the strain rate of 5.808×10^{-5} (sec^{-1}) for the $Zr_{50}Cu_{40}Al_{10}$ metallic glass ribbon. These values are closer that what we observe through direct observation of initiation of shear band for $Fe_{79.3}B_{16.4}Si_4C_{0.3}$ and $Zr_{50}Cu_{40}Al_{10}$ metallic glass ribbons.

3.2.2. Structural variation and shear band evolution under indentation test

In order to observe structural variation depends on the metallic glasses

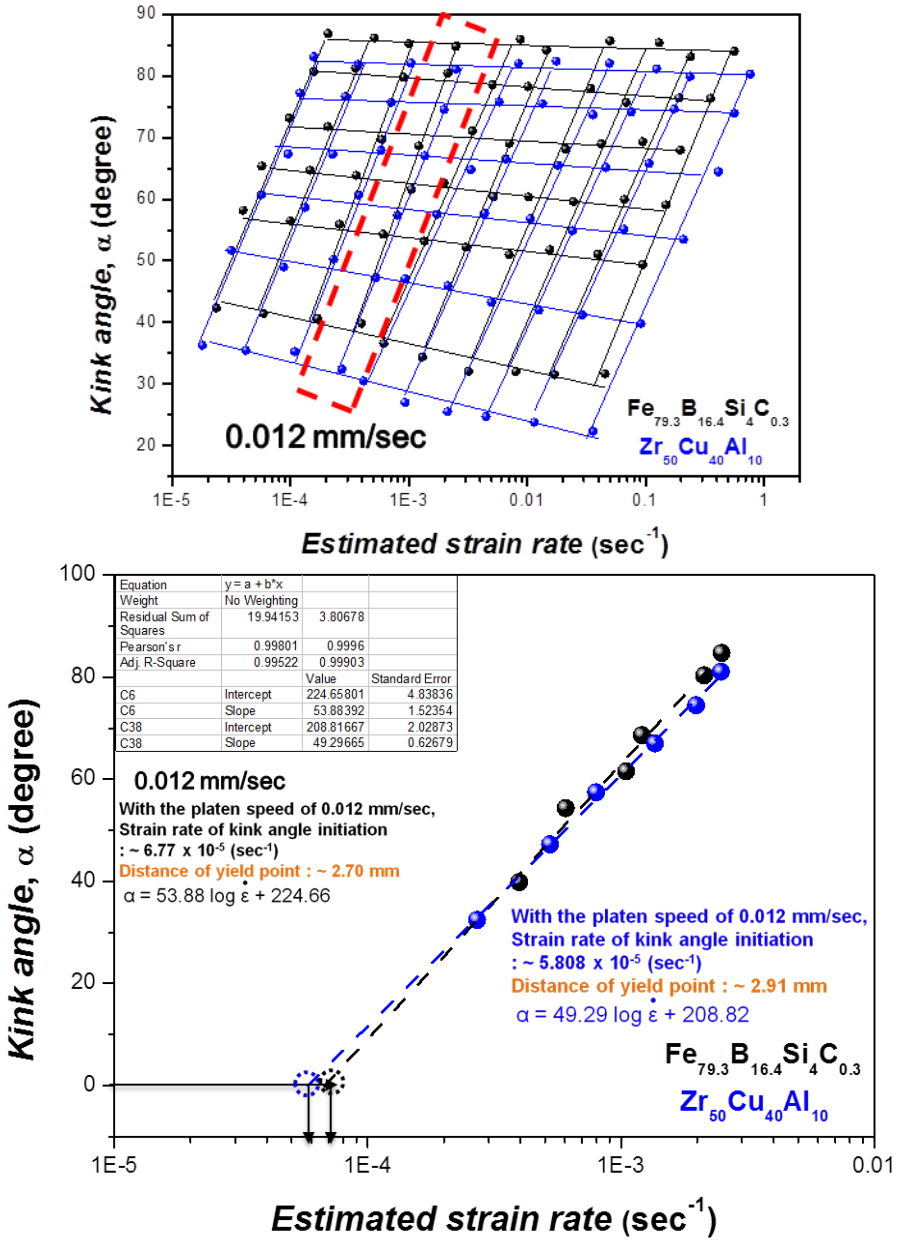

Figure 3.15. Approximation of shear band initiation point by extrapolating the relation between kink angle and estimated strain rate to kink angle initiation point (kink angle = 0) at speed of 0.012 mm/sec for $Fe_{79.3}B_{16.4}Si_4C_{0.3}$ and $Zr_{50}Cu_{40}Al_{10}$ metallic glasses.

(brittle or ductile) a nano indentation test was applied to $Zr_{52.5}Al_{10}Ti_5Cu_{17.9}Ni_{14.6}$ bulk metallic glass [35]. Under 3-point bending test it was observed that the as cast bulk metallic glass ($Zr_{52.5}Al_{10}Ti_5Cu_{17.9}Ni_{14.6}$) shows the plasticity, while the same bulk metallic glass annealed at 300 ^oC shows the brittle fracture, as can see in load-deflection curve under 3-point bending test in figure 3.16. The fracture surface of as cast and annealed (at 300 ^oC) samples were observed under scanning electronic microscope after 3-point bending test as can see in figure 3.16. The fracture surface of as cast sample shows the vein patterns which is the indication of ductile manner while the annealed sample shows the mirror like features because of brittle nature. For the structural heterogeneity observation of as-cast (ductile) and annealed (brittle) bulk metallic glasses a nano-indentation test (Nano-indenter XP system equipped with spherical indenter having radius (R) of 1.78 um) used. A representative load-displacement curve with first pop-in event (indication of onset plastic deformation) and Hertzian solution shown in figure 3.17. A first pop-in point clearly can see on load-displacement curve, which shows the onset plasticity, while Hertzian solution (calculated by below equation) which represent the elastic part of nano-indentation curve, clearly demonstrate the plasticity point in bulk metallic glass through pop-in event as load-displacement curve deviate from elastic part (Hertzian solution) at pop-in point. Hertzian equation is;

$$P = \frac{4}{3} E_r \sqrt{R}\, h^{3/2}$$

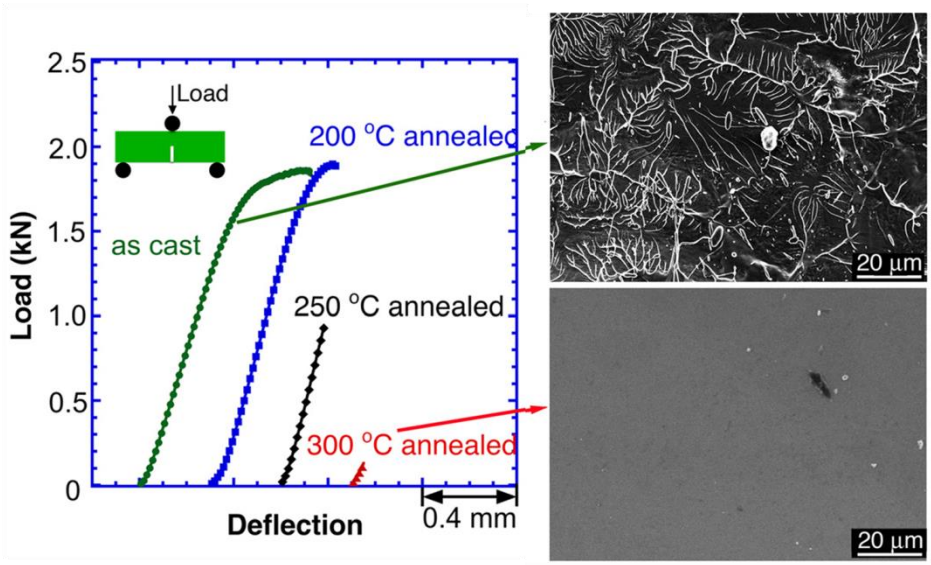

Figure 3.16. Load-deflection curve under 3-point bending test and SEM images of fractured surfaces, of as cast and annealed ($Zr_{52.5}Al_{10}Ti_5Cu_{17.9}Ni_{14.6}$) bulk metallic glass [35].

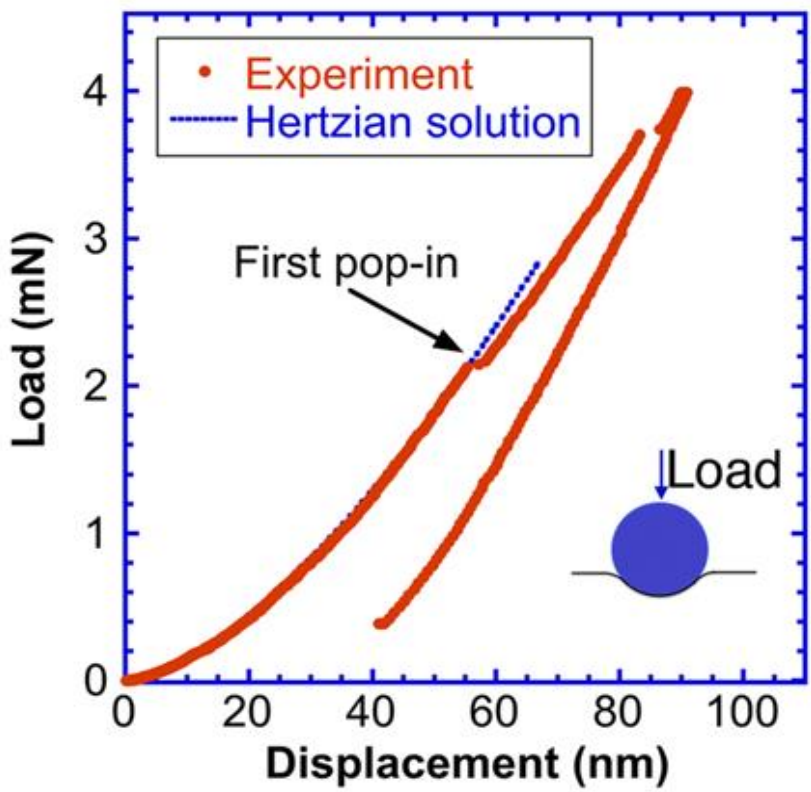

Figure 3.17. Load-displacement curve of as-cast ($Zr_{52.5}Al_{10}Ti_5Cu_{17.9}Ni_{14.6}$) bulk metallic glass at radius of 1.78 μm, represent the pop-in event and Hertzian solution [35].

Where Er is reduced modulus, R is indenter radius, P is load and h is displacement. The maximum shear strength at first pop-in point was calculated by below equation.

$$\tau_{max} = 0.445\ (\frac{16P_{pop-in}}{9\pi^3 R^2} E_r^2\ )^{1/3}$$

Where τ_{max} is maximum shear strength at first pop-in point, Er is reduced modulus R is indenter radius, $P_{pop\text{-}in}$ is load at pop-in and π is constant which is around 3.14. The relationship between maximum shear strength at pop-in and cumulative probability for as cast and annealed samples at radius of 1.78 μm (~1.8 μm) were calculated as shown in figure 3.18. By using this relation a fitting parameters v* (free volume) and ρ_{def} (defect density or soft zone density) were calculated for as-cast and annealed samples as shown in below table 3.2 and figure 3.19. It can be see that the v* and ρ_{def} which help to initiation of shear bands reduces with the annealing of as-cast sample. That is why annealed sample has higher τ_{max} as compared to as-cast sample and it shows brittle fracture under 3-point bending test. While the generation of shear band is much easier in as-cast sample because of higher soft zone density, so it has less τmax for pop-in point and that is why it shows higher ductility under 3-point bending test.

By following above literature, a nano-indentation test were applied to brittle ($Fe_{79.3}B_{16.4}Si_4C_{0.3}$) and ductile ($Zr_{50}Cu_{40}Al_{10}$) metallic glasses. A representative load-displacement curve of $Fe_{79.3}B_{16.4}Si_4C_{0.3}$ metallic glass

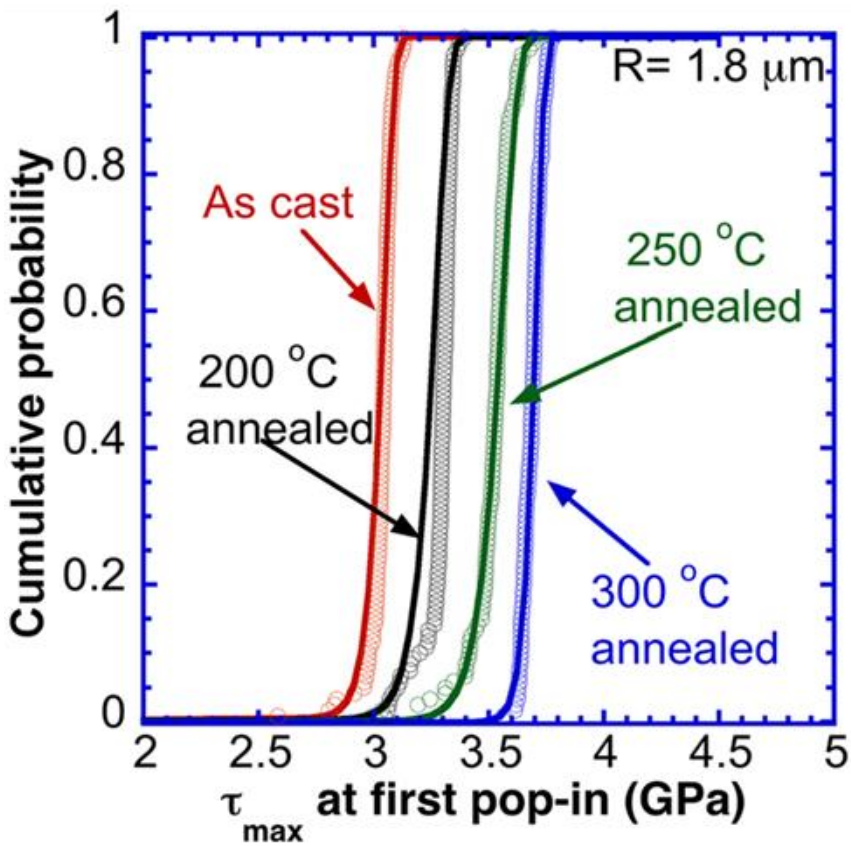

Figure 3.18. Relation between cumulative probability vs τ_{max} at pop-in for as-cast and annealed samples at the radius of 1.8 μm.

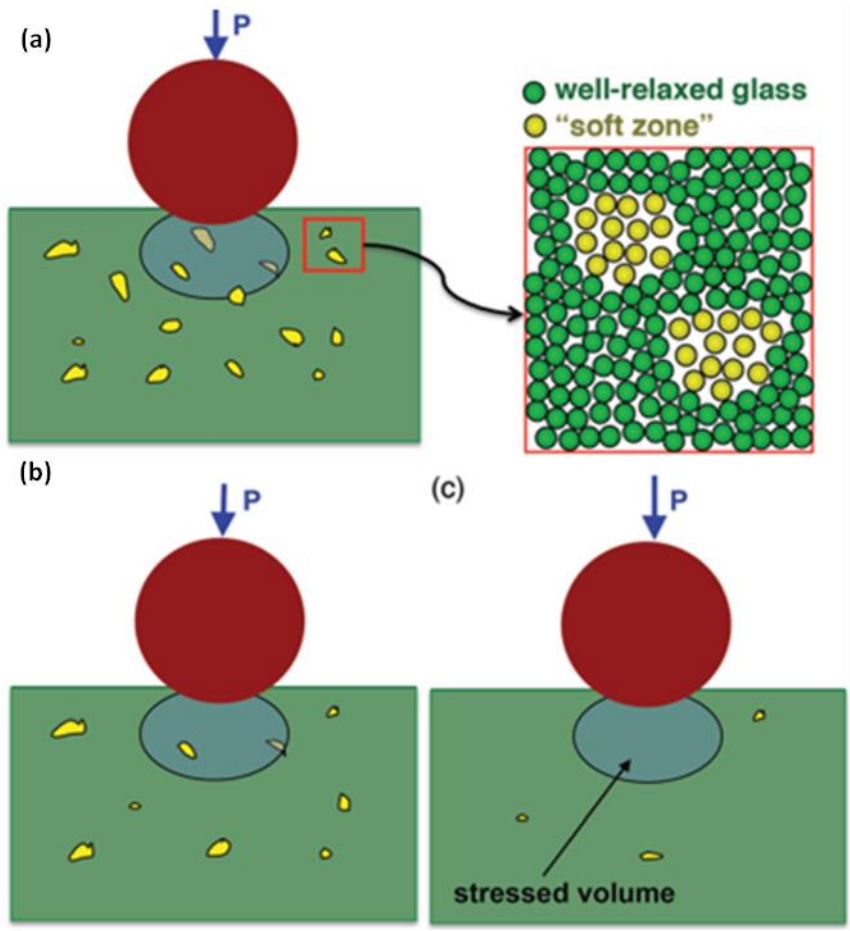

Figure 3.19. The presence of soft zones in as-cast (a) and annealed ((b) half annealed, (c) fully annealed) samples [35].

Indenter radius R (μm)	1.78			
Temperature (°C)	As cast	200	250	300
v* (nm^3)	0.072	0.067	0.062	0.061
ρ_{def} (x 10^{15} m^{-3})	5.40	3.04	1.24	0.11

Table 3.2. Fitting parameters v* and ρ_{def} calculated from load-displacement curve under nano-indentation test [35].

with indenter radius of 1.56 μm shown in figure 3.20 (a). It clearly shows the first pop-in point, while Hertzian curve was also drawn for comparison. The τ_{max} was calculated by using above equation and relation between τ_{max} versus cumulative probability was drawn for brittle and ductile metallic glasses as shown in 3.20 (b). Fitting parameters v* and ρ_{def} were calculated for both alloy systems by using figure 3.20 (b), and shown in table 3.3. It can be seen that the results for brittle ($Fe_{79.3}B_{16.4}Si_4C_{0.3}$) and ductile ($Zr_{50}Cu_{40}Al_{10}$) metallic glasses under nano-indentation test shows the same behavior as in the literature. Because of less free volume and soft-zone density in brittle ($Fe_{79.3}B_{16.4}Si_4C_{0.3}$) metallic glass, the shear band generated at smaller distance between plates under bending test and causes the higher kink angle, because higher shear strength needed to generate shear band under bending and indentation tests. While in ductile ($Zr_{50}Cu_{40}Al_{10}$) metallic glass the shear band generated at larger distance between plates under bending test, because of higher soft zone density and free volumes shear band initiated at lower shear strength.

Similarly shear bands was observed under micro-indentation test. Under micro-indentation at 200gram of load, the shear bands of brittle ($Fe_{79.3}B_{16.4}Si_4C_{0.3}$) and ductile ($Zr_{50}Cu_{40}Al_{10}$) metallic glasses are observed by SEM, as can seen in figure 3.21. It can be seen that the scale pile-up shear bands around $Fe_{79.3}B_{16.4}Si_4C_{0.3}$ metallic glass indentation are less as compared to $Zr_{50}Cu_{40}Al_{10}$ metallic glass indentation. Because of less soft zone density in $Fe_{79.3}B_{16.4}Si_4C_{0.3}$ metallic glass, it has higher resistance against indentation load and it causes few scale pile-up shear bands around

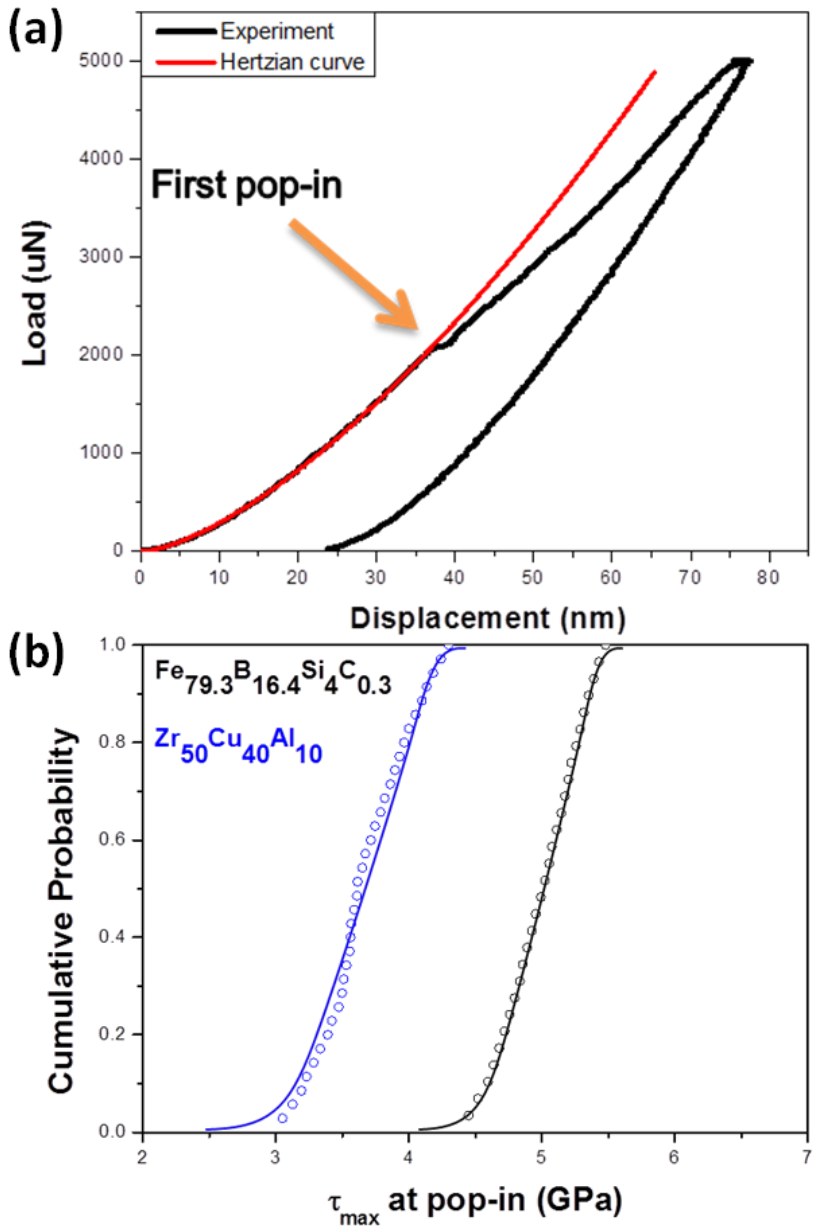

Figure 3.20. (a) A representative load-displacement curve of $Fe_{79.3}B_{16.4}Si_4C_{0.3}$ metallic glass under nano-indentation at radius of 1.56 μm. (b) The relation between τmax and cumulative probability for brittle ($Fe_{79.3}B_{16.4}Si_4C_{0.3}$) and ductile ($Zr_{50}Cu_{40}A_{10}$) metallic glasses.

Alloys	v* (nm^3)	ρ_{def} (x 10^{15} m^{-3})
$Fe_{79.3}B_{16.4}Si_4C_{0.3}$	0.0492	2.959
$Zr_{50}Cu_{40}Al_{10}$	0.0892	5.125

Table 3.3. Fitting parameters v* and ρ_{def} calculated from relation between τ_{max} and cumulative probability under nano-indentation test for $Fe_{79.3}B_{16.4}Si_4C_{0.3}$ and $Zr_{50}Cu_{40}Al_{10}$ metallic glasses.

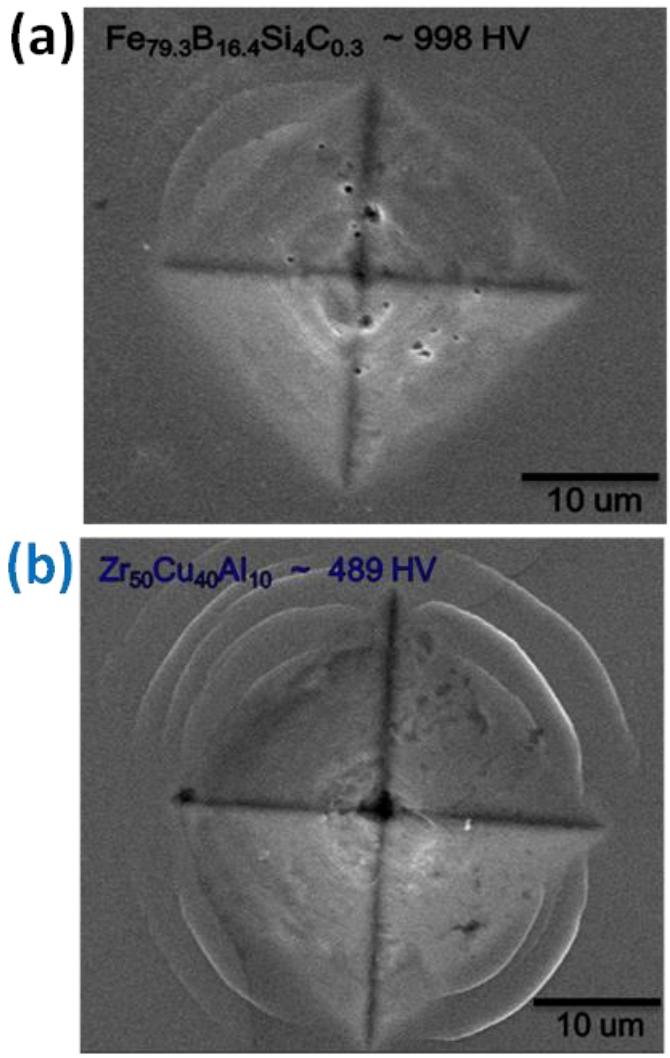

Figure 3.21. Shear band observation by SEM for brittle, $Fe_{79.3}B_{16.4}Si_4C_{0.3}$ (a) and ductile $Zr_{50}Cu_{40}A_{10}$ (b) metallic glasses after micro-indentation test at load of 200 gram.

indenter. While because of higher soft zone density in $Zr_{50}Cu_{40}Al_{10}$ metallic glass, the resistance to indenter load decreases and it causes multiple generation of scale pile-up shear bands around indenter. The micro-hardness and nano-hardness values for brittle ($Fe_{79.3}B_{16.4}Si_4C_{0.3}$) and ductile ($Zr_{50}Cu_{40}Al_{10}$) metallic glasses are shown in below table 3.4. Because of different density of scale pile-up shear bands the hardness value of brittle metallic glass is higher as compared to ductile metallic glass and also it noted that the hardness value decreases at higher load for both compositions.

3.3. Comparison between strong and fragile metallic glasses depending on Zr-based alloy system

In this part, variation of kink angle for strong glass former ($Zr_{50}Cu_{40}Al_{10}$) and fragile glass former ($Zr_{60}Cu_{30}Al_{10}$) were explained. The strong glass former has higher glass forming ability as compared to fragile glass former as explained in section 1.2.1. The other properties of strong and fragile glass formers were mentioned in table 3.5 [36]. It was noticed that the space among the constituent elements of strong glass former is less due to high glass forming ability and high viscosity as compared to fragile glass former. Because of the less space among the constituent elements of strong glass former, the bond among the constituent elements is strong which cause the higher yield strength and low plasticity of strong glass former. While in case of fragile glass former, the space

Micro-Indentation	100 gram	200 gram	Nano-Indentation
$Fe_{79.3}B_{16.4}Si_4C_{0.3}$	~ 1017 HV	~ 998 HV	~ 10.14 GPa
$Zr_{50}Cu_{40}Al_{10}$	~ 558 HV	~ 489 HV	~ 6.98 GPa

Table 3.4. Micro-hardness and nano-hardness values for brittle ($Fe_{79.3}B_{16.4}Si_4C_{0.3}$) and ductile ($Zr_{50}Cu_{40}Al_{10}$) metallic glasses.

among the constituent elements is higher and it helps to easy initiation of shear bands because of easy movement of atoms (free volume creation) and ultimately higher plasticity as compared to strong glass former but it gives lower yield strength. The shear bands were observed for strong and fragile glass formers after bending fatigue test and it noticed that the shear band density for fragile glass former is higher than strong glass former. The shear band morphology of these two compositions is shown in figure 3.22 [19].

3.3.1. Shear band evolution under bending test depending on kink angle variation

The relation between kink angle and estimated strain rate for strong metallic glass ($Zr_{50}Cu_{40}Al_{10}$) alloy and fragile metallic glass ($Zr_{60}Cu_{30}Al_{10}$) alloy were also calculated as shown in figure 3.23. It noted that the strong metallic glass has the higher kink angle while the fragile metallic glass has the lower kink angle. Because of the low yield strength of fragile metallic glass as compared to strong metallic glass, the shear band initiated at larger distance between plates as compared to strong metallic glass and this cause the low kink angle. The deformed region of these two alloys were observed under SEM after bending test at the distance of 1.1 mm between plates and at the speed of 0.001 mm/sec of moving plate which give the kink angle of 36.277^{o} for strong metallic glass ($Zr_{50}Cu_{40}Al_{10}$) and 35.286^{o} for fragile

Composition	Glass forming ability	Poisson ratio	Plasticity	Young Modulus	Fracture strength	Casting diameter of BMG
$Zr_{50}Cu_{40}Al_{10}$	Higher	0.363	Lower	88 GPa	1821 MPa	22 mm
$Zr_{60}Cu_{30}Al_{10}$	Lower	0.373	Higher	80 GPa	1720 MPa	8 mm

Table 3.5. Physical properties of strong and fragile glass formers [36].

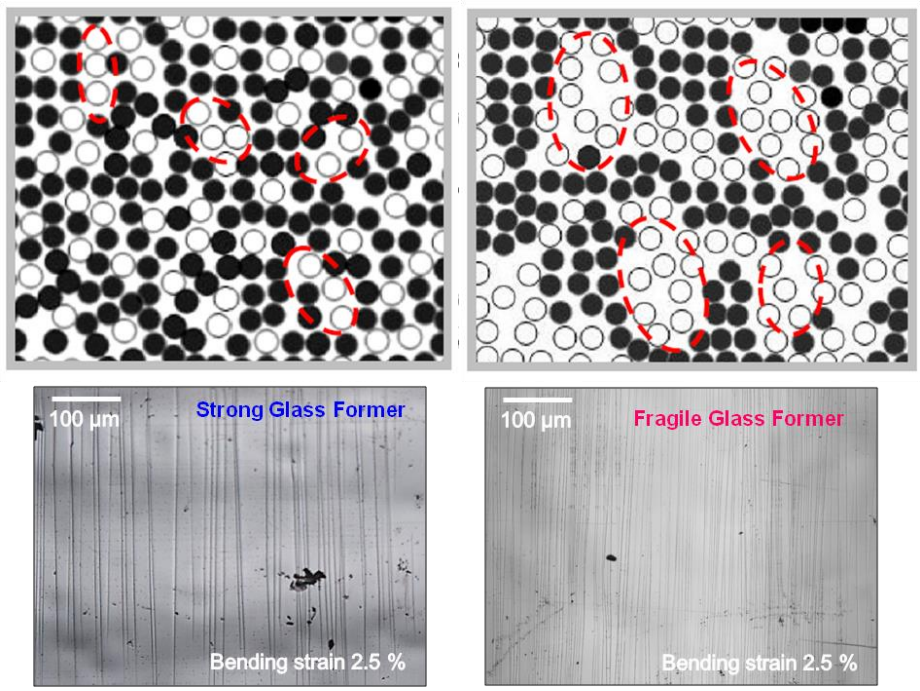

Figure 3.22. Schematic diagrams and shear bands morphology of strong glass former ($Zr_{50}Cu_{40}Al_{10}$) at left side and fragile glass former ($Zr_{60}Cu_{30}Al_{10}$) at right side [19].

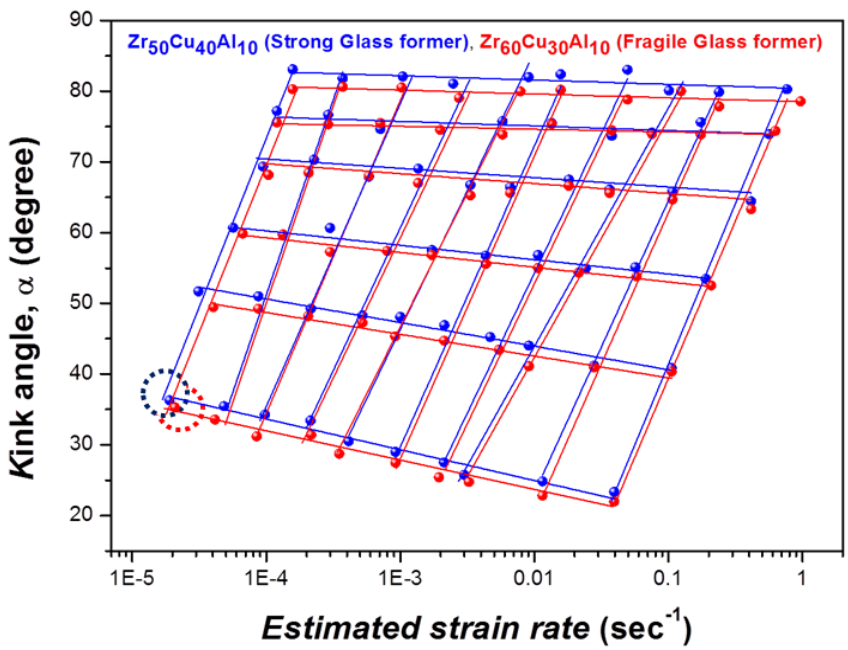

Figure 3.23. Relation between kink angle and estimated strain rate for strong metallic glass ($Zr_{50}Cu_{40}Al_{10}$) alloy and fragile metallic glass ($Zr_{60}Cu_{30}Al_{10}$) alloy under bending test.

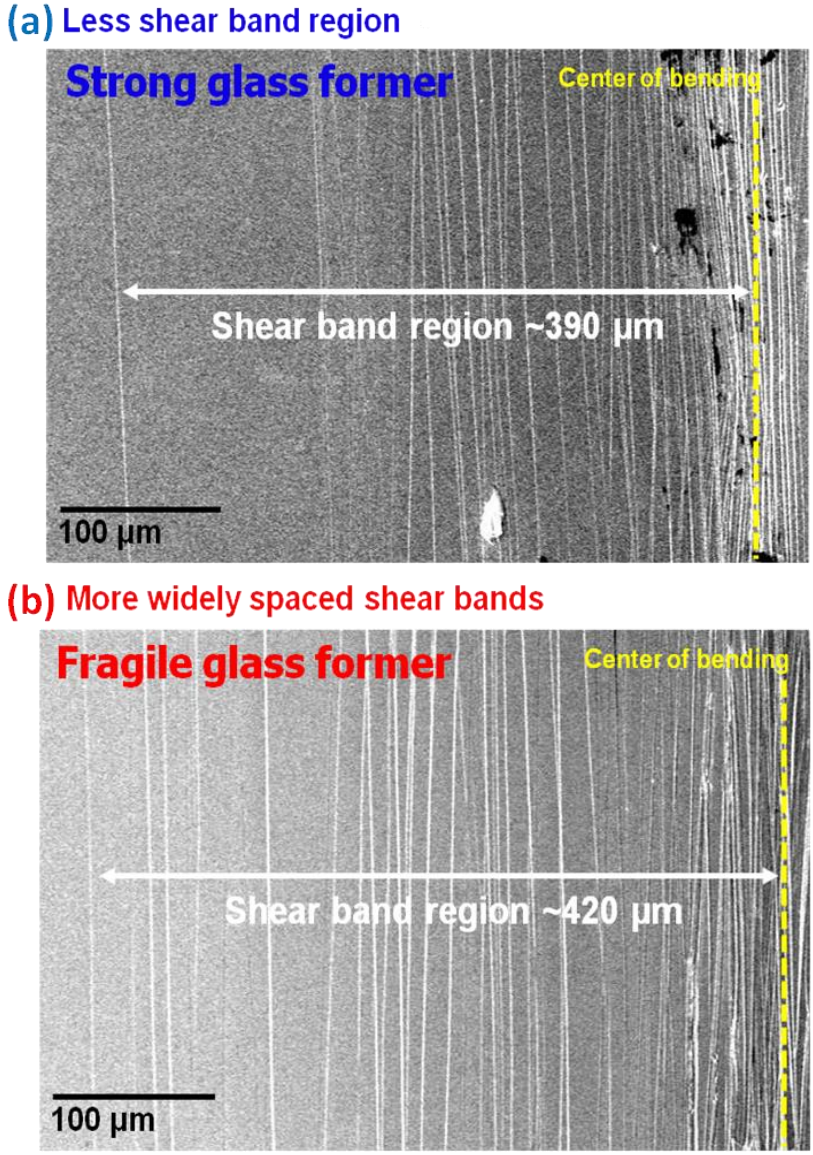

Figure 3.24. SEM images of $Zr_{50}Cu_{40}Al_{10}$ (a) and $Zr_{60}Cu_{30}Al_{10}$ (b) metallic glasses, which measured at distance of 1.1 mm between plates with speed of 0.001 mm/sec of moving plate and it gives kink angle of 36.277^{o} for $Zr_{50}Cu_{40}Al_{10}$ (blue circle at figure 3.19) and 35.286^{o} for $Zr_{60}Cu_{30}Al_{10}$ (red circle at figure 3.19)metallic glasses.

metallic glass ($Zr_{60}Cu_{30}Al_{10}$). By SEM observation of shear band region of Zr based alloys as can see in figure 3.24, it was noted that $Zr_{50}Cu_{40}Al_{10}$ metallic glass has concentrated shear bands with the shear band region of 390 μm, while the shear band region is higher for fragile metallic glass ($Zr_{60}Cu_{30}Al_{10}$), which has shear band region around 420 μm with widely spaced shear bands and less concentrated shear bands at center as compared to other alloy. The concentrated shear bands at small region cause the more deformation at center and it has less recovery after bending test as in case of $Zr_{50}Cu_{40}Al_{10}$ metallic glass and it shows higher kink angle, while the widely spaced shear bands has less deformed region at center and it causes more recovering after bending test and it has lower kink angle as in case of fragile metallic glass ($Zr_{60}Cu_{30}Al_{10}$). These results are similar of section 3.2.1 for brittle and ductile metallic glasses.

3.3.2. Structural variation and shear band evolution under indentation test

In order to observe structural variation of Zr based alloys system, a nano-indentation test was used similar as for brittle and ductile metallic glasses in section 3.2.2. The relation between maximum shear strength at pop-in and cumulative probability for strong metallic glass ($Zr_{50}Cu_{40}Al_{10}$) alloy and fragile metallic glass ($Zr_{60}Cu_{30}Al_{10}$) alloy shown in figure 3.25. By using figure 3.25, fitting parameters v* and ρ_{def} were calculated as shown in below table 3.6. It can be seen that $Zr_{60}Cu_{30}Al_{10}$ has the higher

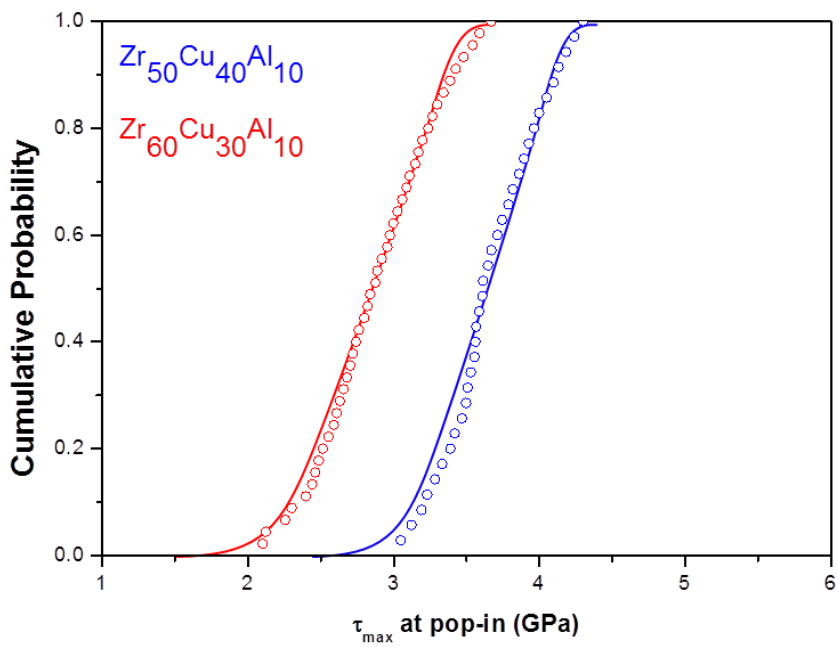

Figure 3.25. The relation between τ_{max} and cumulative probability for strong metallic glass ($Zr_{50}Cu_{40}Al_{10}$) alloy and fragile metallic glass ($Zr_{60}Cu_{30}Al_{10}$) alloy.

Alloys	v* (nm^3)	ρ_{def} (x 10^{15} m^{-3})
$Zr_{50}Cu_{40}Al_{10}$	0.0892	5.125
$Zr_{60}Cu_{30}Al_{10}$	0.0997	6.013

Table 3.6. Fitting parameters v* and ρ_{def} calculated from relation between τ_{max} and cumulative probability under nano-indentation test for Zr based alloys system.

activation volume and soft zone density while $Zr_{50}Cu_{40}Al_{10}$ has the lower activation volume and soft zone density. Because of higher soft zone density in $Zr_{60}Cu_{30}Al_{10}$, it has higher chances to generate shear bands easily as compared to other alloy and initiation of shear band happened at lower shear stress. Because of higher activation volume and soft zone density in $Zr_{60}Cu_{30}Al_{10}$ metallic glass, the shear bands initiated at larger distance between plates and it causes the widely spaced shear bands in a larger region instead of concentrated shear bands at small region and this cause the larger recovering of bended sample which ultimately gives low kink angle as compared to strong metallic glass which has higher kink angle due to concentrated shear bands at center and less recovering curvature after removing bending forces.

Micro-hardness test was applied to Zr based alloys, in order to know their shear band morphology under indentation. At 100 gram load both the Zr based alloys show the scale pile up shear bands around indenter with different density, while at 200 gram load strong metallic glass ($Zr_{50}Cu_{40}Al_{10}$) alloy shows scale pile-up shear bands but fragile metallic glass ($Zr_{60}Cu_{30}Al_{10}$) alloy fractured at the same load. The shear bands morphology at 100 and 200 gram loads for both Zr based alloys shown in figure 3.26 which observed under SEM after indentation test. It noted that because of low soft zone density in $Zr_{50}Cu_{40}Al_{10}$ metallic glass, it has higher resistance against indentation load and that's why it has fewer scale pile-up shear bands as compared to other alloy. But in case of fragile metallic glass ($Zr_{60}Cu_{30}Al_{10}$), due to high free volume and soft zone density, it has lower

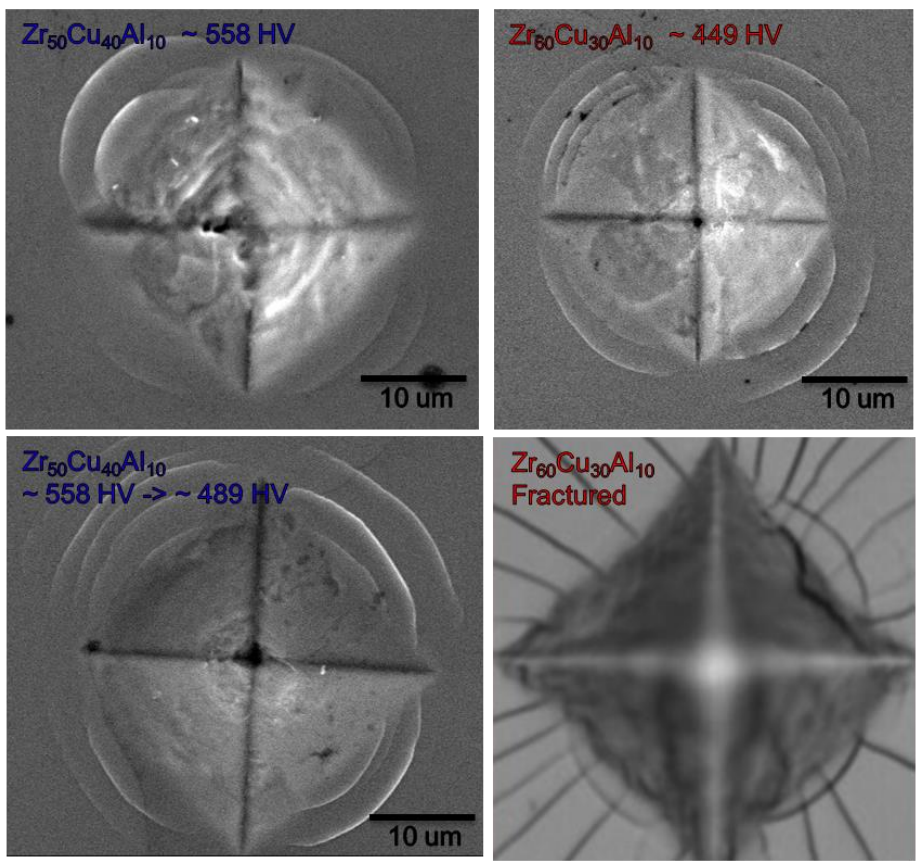

Figure 3.26. Shear bands observation by SEM for $Zr_{50}Cu_{40}Al_{10}$ (left) and $Zr_{60}Cu_{30}Al_{10}$ (right) metallic glasses after micro-indenation test at load of 100 gram (top row) and 200 gram (below row).

Micro-Indentation	100 gram	200 gram	Nano-Indentation
$Zr_{50}Cu_{40}Al_{10}$	~ 558 HV	~ 489 HV	~ 6.98 GPa
$Zr_{60}Cu_{30}Al_{10}$	~ 449 HV	Fractured	~ 5.54 GPa

Table 3.7. Micro-hardness and nano-hardness values for strong metallic glass ($Zr_{50}Cu_{40}Al_{10}$) alloy and fragile metallic glass ($Zr_{60}Cu_{30}Al_{10}$) alloy.

resistance against indentation load as compared to other alloy, as can see that it has higher scale pile-up shear bands at 100 gram load while it fracture at 200 gram load because of lowest resistance against indentation. The micro-hardness and nano- hardness values for Zr based alloys are shown in below table 3.7. Hardness values varied depends on the composition and load. The scale pile-up shear bands are higher for lower hardness value. The hardness value was calculated in literature for Zr based alloy bulk metallic glasses and it noted that $Zr_{50}Cu_{40}Al_{10}$ bulk metallic glass has 496 HV hardness value and $Zr_{60}Cu_{30}Al_{10}$ bulk metallic glass has hardness value of 446 HV [37]. The hardness values for current research ribbons case are almost similar as mentioned in literature for bulk metallic glasses. As $Zr_{50}Cu_{40}Al_{10}$ metallic glass has 499 HV hardness value at 200 gram of load. While $Zr_{60}Cu_{30}Al_{10}$ metallic glass has 449 HV hardness value at 100 gram load.

3.4. Comparison of phase separating metallic glasses depending on heterogeneity size

In this part, deformation behavior of phase separating metallic glasses explained with the help of kink angle variation. It was noticed that Cu-Zr-Al alloy has the negative heat of mixing among the elements but the addition of yttrium cause the positive heat of mixing with Zr element which basis the phase separating of metallic glass (as explained in section 1.2.2). As addition of yttrium in Cu-Zr-Al system form two amorphous phases, Zr-Cu-

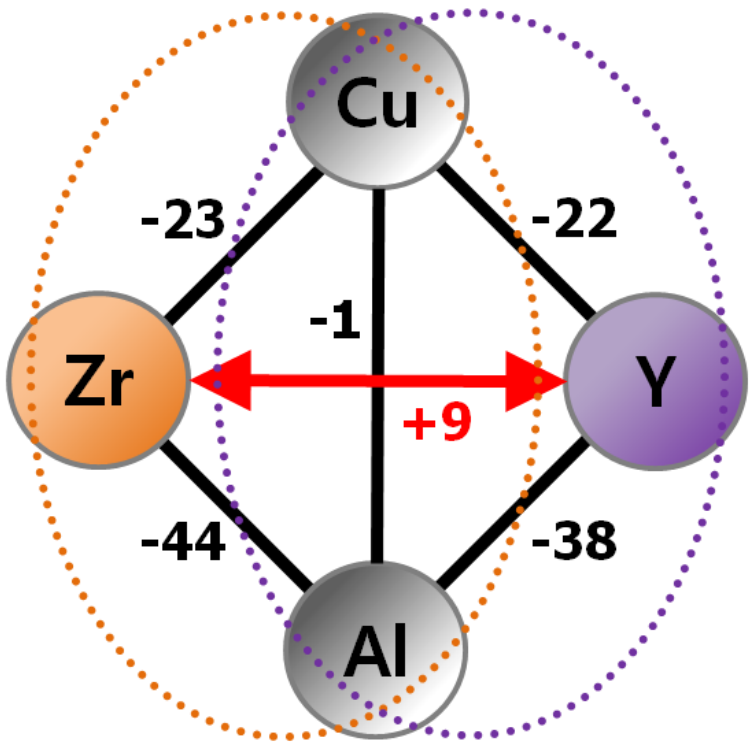

Figure 3.27. Heat of mixing relations in Cu-Zr-Al-Y alloy system [17].

rich and Y-Cu-rich phases. The heat of mixing relations in Cu-Zr-Al-Y alloy system shown in below figure 3.27 [17]. To detect heterogeneity visually, the microstructure of alloy with 5 at.% Y was observed by TEM, but there is no detected heterogeneity within TEM resolution in as-cast alloy while we can observe nanocrystals when the alloy is annealed at 480 celcius. From this, we can suggest the presence of atomic scale heterogeneity inside as-spun Y5 ribbon sample. The TEM images shown in figure 3.28 [17]. So this shows that more addition of yttrium causes phase separation as noticed in Y10 or higher [17]. In this research $Cu_{46}Zr_{47-x}Al_7Y_x$ (x= 0, 5, 10) alloys used in order to know their deformation behavior. The physical properties of $Cu_{46}Zr_{47-x}Al_7Y_x$ (x= 0, 5, 10) alloys shown in table 3.8 [38].

3.4.1. Shear bands evolution under bending test depending on kink angle variation

A bending test was also applied to phase separating metallic glasses, in order to know their mechanical properties. It was noted that with the addition of yttrium, kink angle of $Cu_{46}Zr_{47-x}Al_7Y_x$ (x= 0, 5, 10) alloy series decreases as shown in below figure 3.29.

The shear bands morphology was observed under SEM after bending test at a distance of 1.1 mm between plates with speed of 0.001 mm/sec of moving plate, which give kink angle value of 40.188^o for $Cu_{46}Zr_{47}Al_7Y_0$ alloy, 38.999^o for $Cu_{46}Zr_{42}Al_7Y_5$ alloy and 36.659^o for $Cu_{46}Zr_{37}Al_7Y_{10}$ alloy as shown in figure 3.30. It can be noted that $Cu_{46}Zr_{47}Al_7Y_0$ has concentrated

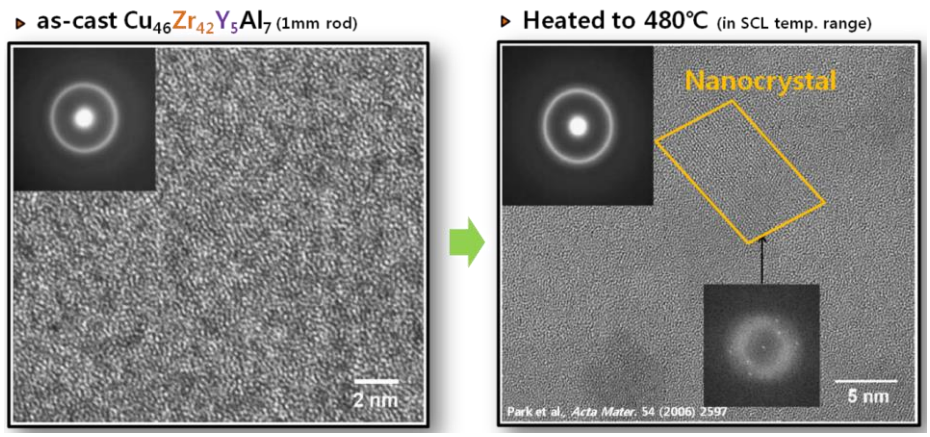

Figure 3.28. Atomic scale heterogeneity in Y5 by indirect evidence from TEM. It clearly shows that nanocrystallization occurred in SCL region prior to obvious crystallization [17].

Composition	Fracture strength	Young modulus
$Cu_{46}Zr_{47}Al_7Y_0$	1960 MPa	1070 MPa
$Cu_{46}Zr_{42}Al_7Y_5$	1750 MPa	1020 MPa
$Cu_{46}Zr_{37}Al_7Y_{10}$	1640 MPa	960 MPa

Table 3.8. Physical properties of $Cu_{46}Zr_{47-x}Al_7Y_x$ (x= 0, 5, 10) alloys [38].

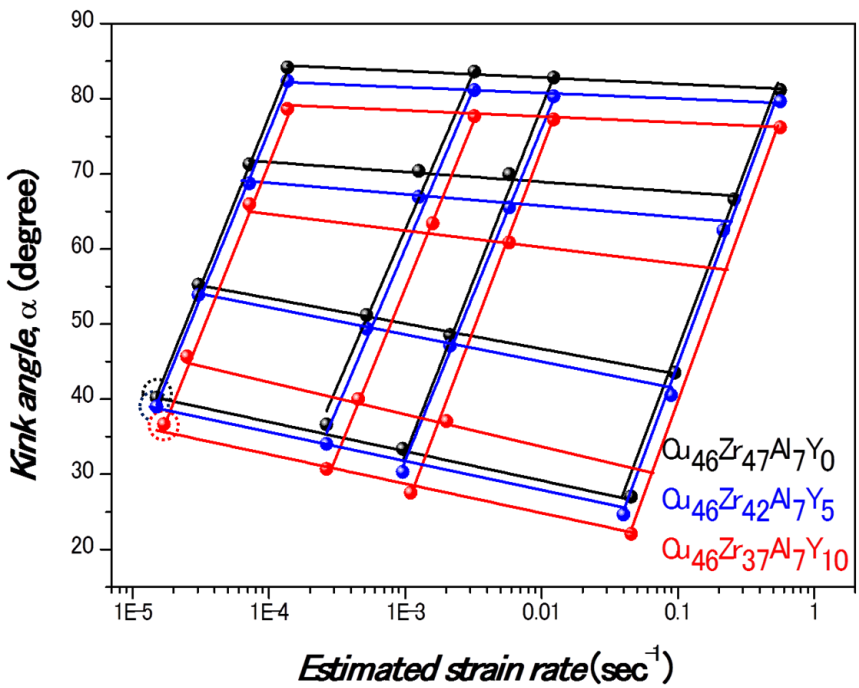

Figure 3.29. Relation between kink angle and estimated strain rate for $Cu_{46}Zr_{47-x}Al_7Y_x$ (x= 0, 5, 10) alloy series under bending test.

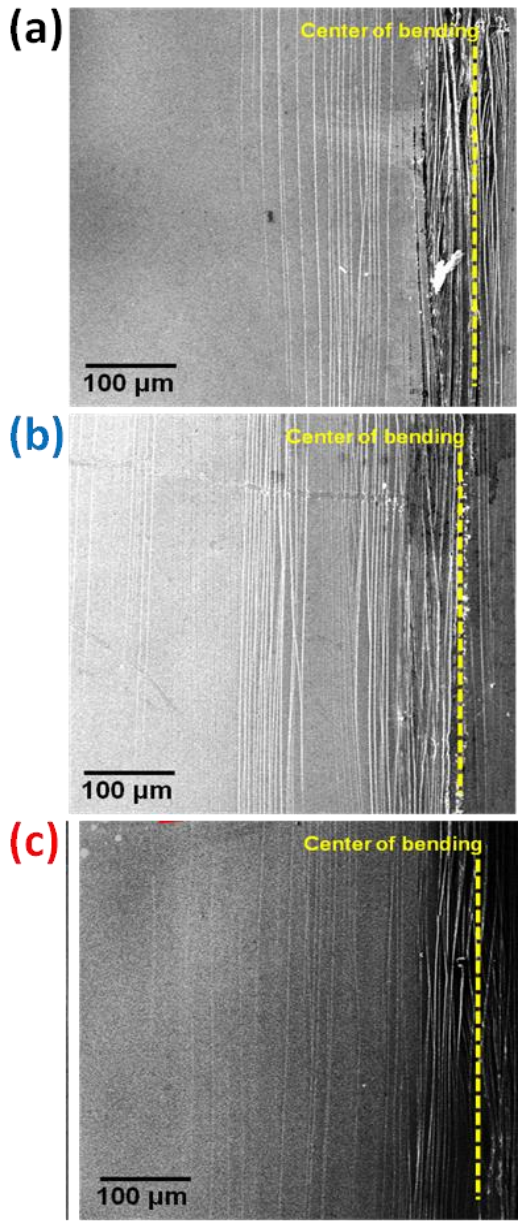

Figure 3.30. SEM images of $Cu_{46}Zr_{47-x}Al_7Y_x$ (x= 0 (a), 5 (b), 10 (c)) alloy series, which measured at distance of 1.1 mm between plates with speed of 0.001 mm/sec of moving plate and it gives kink angle of 40.188° for $Cu_{46}Zr_{47}Al_7Y_0$ alloy (black circle at figure 3.29), 38.999° for $Cu_{46}Zr_{42}Al_7Y_5$ alloy (blue circle at figure 3.29) and 36.659° for $Cu_{46}Zr_{37}Al_7Y_{10}$ alloy (red circle at figure 3.29).

shear bands with small shear band region as compared to $Cu_{46}Zr_{42}Al_7Y_5$ and $Cu_{46}Zr_{37}Al_7Y_{10}$, which have large number of shear bands in a widely spaced region. Because of concentrated shear bands in a small region, $Cu_{46}Zr_{47}Al_7Y_0$ has a less recovering curvature after bending test and it causes the higher kink angle as compared to other two alloys. The addition of yttrium causes the more shear bands generation and it has widely spaced shear band region instead of concentrated shear bands at center and this cause less deformation at center and more recovering after removal bending forces which gives low kink angle. The $Cu_{46}Zr_{42}Al_7Y_5$ alloy has higher shear band density with large shear band region as compared to $Cu_{46}Zr_{37}Al_7Y_{10}$ alloy, which has less shear band region with fewer shear bands but still $Cu_{46}Zr_{42}Al_7Y_5$ alloy shows higher kink angle, which because of intrinsic ductility of $Cu_{46}Zr_{37}Al_7Y_{10}$ alloy. Even though $Cu_{46}Zr_{37}Al_7Y_{10}$ alloy don't show higher shear band density as compared to $Cu_{46}Zr_{42}Al_7Y_5$ alloy, but still it shows lower kink angle which may be due to generation of more shear bands intrinsically that don't show up on the surface and this cause the higher recovering curvature as compared to $Cu_{46}Zr_{42}Al_7Y_5$ alloy. By considering the center region of both alloys ($Cu_{46}Zr_{42}Al_7Y_5$ and $Cu_{46}Zr_{37}Al_7Y_{10}$), it can be noticed that $Cu_{46}Zr_{42}Al_7Y_5$ alloy has higher rough deformed region at center as compared to $Cu_{46}Zr_{37}Al_7Y_{10}$ alloy which has only crossed shear bands at center causing more recovery after removal of bending forces.

3.4.2. Structural variation and shear bands evolution under indentation test

For the observation of structural heterogeneity size effect on intrinsic ductility of phase separating metallic glasses a nano-indentation test was applied to $Cu_{46}Zr_{47-x}Al_7Y_x$ (x= 0, 5, 10) alloy series, as shown in figure 3.31. It noted that $Cu_{46}Zr_{47}Al_7Y_0$ alloy has higher τ_{max} at pop-in as compared to other two alloys ($Cu_{46}Zr_{42}Al_7Y_5$ and $Cu_{46}Zr_{37}Al_7Y_{10}$). As $Cu_{46}Zr_{47}Al_7Y_0$ alloy is monolithic, it has only free volume but with the addition of yttrium, the $Cu_{46}Zr_{47}Al_7Y_0$ alloy becomes phase separating and structural heterogeneity occurred with free volume. Because of phase separating nature the resistance between atoms of matrix (constituent elements) and structural heterogeneity increases and it has higher chances to generate shear bands as compared to only free volume in metallic glass. Because $Cu_{46}Zr_{47}Al_7Y_0$ alloy has only free volume, so higher shear strength needed to generated shear band (pop-in point) because it has strong interaction among atoms and that's why it has concentrated shear bands with small shear band region under bending test due to initiation of shear bands at smaller distance between plates and this give higher kink angle as compared to other two alloys because more deformation at center causes less recovering curvature. While in case of $Cu_{46}Zr_{42}Al_7Y_5$ alloy, atomic scale heterogeneity has repulsive interaction with the atoms of matrix (constituent elements) and it needs lower shear strength to generate shear bands and it causes lower deformation at center which gives kink angle lower then $Cu_{46}Zr_{47}Al_7Y_0$ alloy. It noted that $Cu_{46}Zr_{37}Al_7Y_{10}$ alloy, need lowest shear

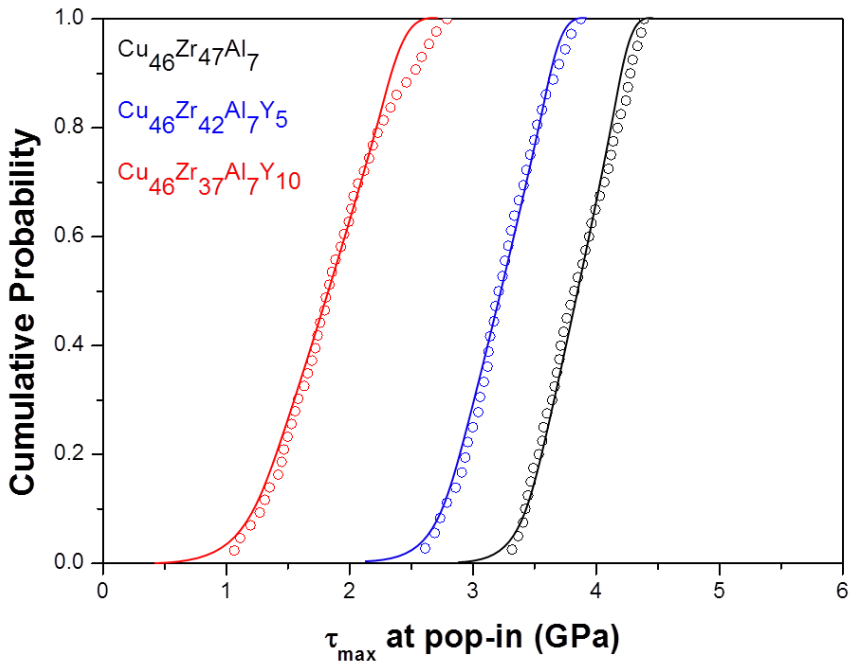

Figure 3.31. The relation between τ_{max} and cumulative probability for $Cu_{46}Zr_{47-x}Al_7Y_x$ (x= 0, 5, 10) alloy series.

strength as compared to other two alloys because in this case nano-scale heterogeneity occurred and repulsion between atoms of matrix (constituent elements) and nano-scale heterogeneity increases more and this cause higher intrinsic ductility as compared to other two alloys which give lower kink angle because of less deformed center region and more recovering after bending test due to initiation of shear bands at larger distance between plates as compared to other two alloys ($Cu_{46}Zr_{47}Al_7Y_0$ and $Cu_{46}Zr_{42}Al_7Y_5$).

Shear bands observation under SEM after micro-indentation test at load of 200 gram was done for $Cu_{46}Zr_{47-x}Al_7Y_x$ (x= 0, 5, 10) alloy series as can see in figure 3.32. It was noted that $Cu_{46}Zr_{47}Al_7Y_0$ alloy has the higher hardness as compared to other two alloys ($Cu_{46}Zr_{42}Al_7Y_5$ and $Cu_{46}Zr_{37}Al_7Y_{10}$) under micro and nano indentation tests as can see in table 3.9. Figure 3.32 clearly shows the difference of scale pile-up shear bands depends upon the alloy composition. As can see that $Cu_{46}Zr_{47}Al_7Y_0$ alloy has the lower scale pile-up shear bands as compared to other two alloys and scale pile-up shear bands increases with the addition of yttrium. Because of presence of only free volume in $Cu_{46}Zr_{47}Al_7Y_0$ alloy, it can resist well against indentation load due to strong interaction among the constituents elements. While in case of $Cu_{46}Zr_{42}Al_7Y_5$ alloy, due to the presence of atomic scale heterogeneity the repulsive interaction among constituent elements and atomic scale heterogeneity reduce the resistance against indentation load and causes the lower hardness with generation of multiple scale pile-up shear bands. Similarly due to increase of repulsive interaction among constituent elements and nano scale heterogeneity in case of

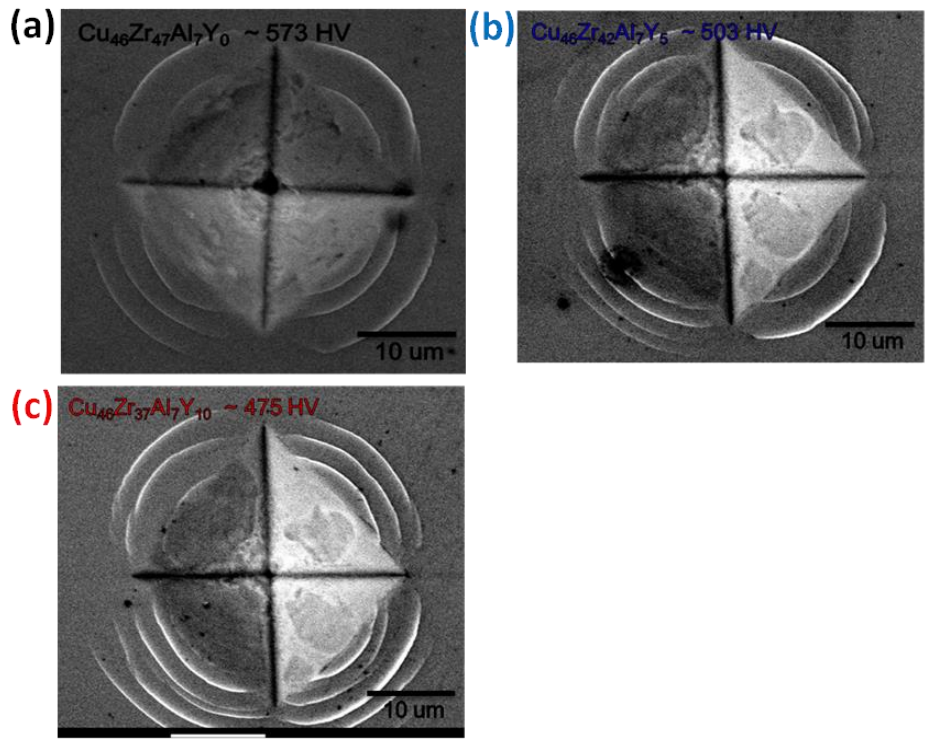

Figure 3.32. Shear bands observation by SEM for $Cu_{46}Zr_{47-x}Al_7Y_x$ (x= 0 (a), 5 (b), 10 (c)) alloy series after micro-indentation test at load of 200 gram.

Composition	200 gram	Nano-Indentation
$Cu_{46}Zr_{47}Al_7Y_0$	~ 573 HV	~ 7.36 GPa
$Cu_{46}Zr_{42}Al_7Y_5$	~ 503 HV	~ 6.76 GPa
$Cu_{46}Zr_{37}Al_7Y_{10}$	~ 475 HV	~ 6.57 GPa

Table 3.9. Micro-hardness and nano-hardness values for $Cu_{46}Zr_{47-x}Al_7Y_x$ (x= 0, 5, 10) alloy series.

$Cu_{46}Zr_{37}Al_7Y_{10}$ alloy, the resistance against indentation load reduces more, as can noticed by higher density of scale pile-up shear bands and lowest hardness as compared to other two alloys.

3.4.3. Fatigue limit under bending fatigue test

A bending fatigue test was applied to $Cu_{46}Zr_{47-x}Al_7Y_x$ (x= 0, 5, 10) alloy series in order to know their strain life-time and fatigue strength [39-42]. A fatigue test was done at different strains and relation between strain versus fatigue lifetime was drawn for $Cu_{46}Zr_{47-x}Al_7Y_x$ (x= 0, 5, 10) alloy series, as can see in figure 3.33. It noticed that strain life time of $Cu_{46}Zr_{47}Al_7Y_0$ alloy is around 0.75 percentage, while 0.51 percentage for $Cu_{46}Zr_{42}Al_7Y_5$ alloy and 0.45 percentage for $Cu_{46}Zr_{37}Al_7Y_{10}$ alloy.

By using Basquin's law (high cycle fatigue), the fatigue strength of $Cu_{46}Zr_{47-x}Al_7Y_x$ (x= 0, 5, 10) alloy series was calculated and relation between stress versus fatigue lifetime was drawn as shown in figure 3.34. It noticed that the fatigue strength of $Cu_{46}Zr_{47}Al_7Y_0$ alloy is around 800 MPa, while 580 MPa for $Cu_{46}Zr_{42}Al_7Y_5$ alloy and 400 MPa for $Cu_{46}Zr_{37}Al_7Y_{10}$ alloy. The fatigue strength data calculated here follows the same trend as other Zr-based metallic glasses under bending fatigue test, as can see in figure 3.35 as represented by dotted rectangle [43]. As explained before, $Cu_{46}Zr_{47}Al_7Y_0$ alloy has only free volume and it has strong interaction among the atoms while with the addition of yttrium the scale heterogeneity occurred in $Cu_{46}Zr_{42}Al_7Y_5$ and $Cu_{46}Zr_{37}Al_7Y_{10}$ alloys which cause the repulsion

interaction among matrix atoms and scale heterogeneity. Because of strong interaction among the atoms in $Cu_{46}Zr_{47}Al_7Y_0$ alloy, the shear band initiation happened at higher number of cycles and also the multiplication of shear bands and propagation not occurred easily for $Cu_{46}Zr_{47}Al_7Y_0$ alloy. While because of scale heterogeneity in $Cu_{46}Zr_{42}Al_7Y_5$ and $Cu_{46}Zr_{37}Al_7Y_{10}$ alloys, the shear band initiation happened at lower number of cycles, and also in these alloys multiple shear bands generate easily and propagate fastly as compared to $Cu_{46}Zr_{47}Al_7Y_0$ alloy. Because of the initiation and propagation of shear bands easily in yttrium contained alloys, it causes the less resistance for the propagation of crack and it gives lower fatigue strength [44].

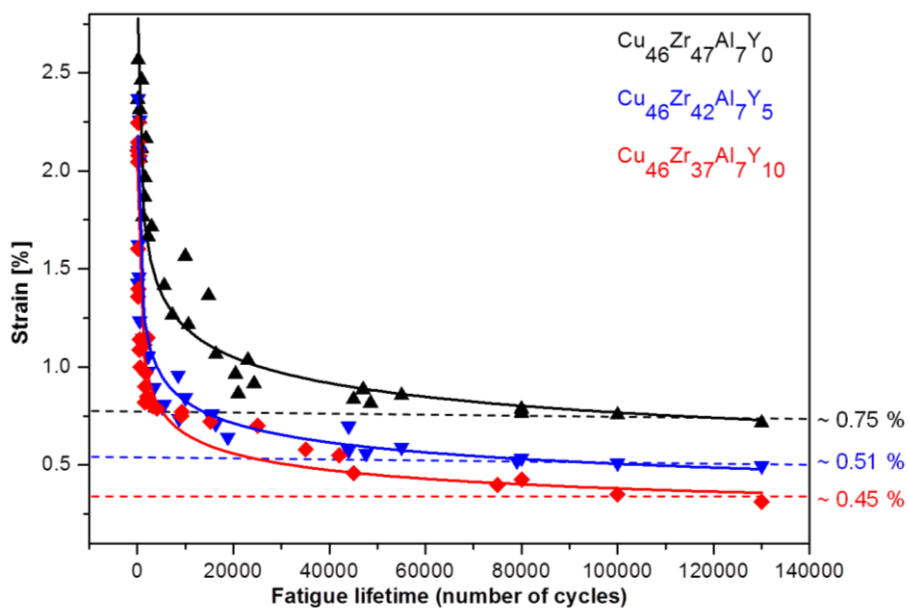

Figure 3.33. Strain-lifetime curves for $Cu_{46}Zr_{47-x}Al_7Y_x$ (x= 0, 5, 10) alloy series after bending fatigue test.

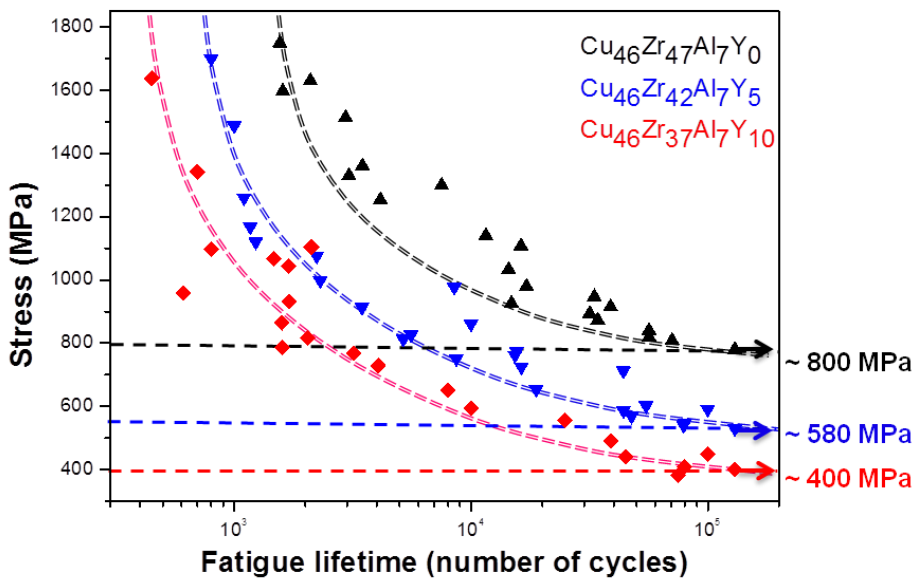

Figure 3.34. Fatigue limit of $Cu_{46}Zr_{47-x}Al_7Y_x$ (x= 0, 5, 10) alloy series after bending fatigue test.

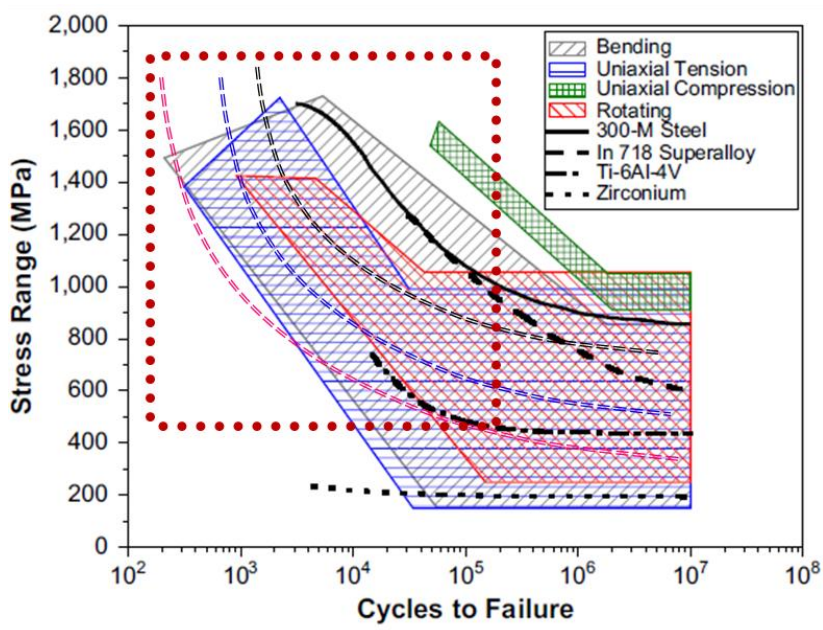

Figure 3.35. Comparison of fatigue limit curve of $Cu_{46}Zr_{47-x}Al_7Y_x$ (x= 0, 5, 10) alloy series after bending fatigue test (as represented by dotted rectangle) and other Zr-based alloys [43].

Chapter 4. Conclusions

1) Plastic deformation in metallic glasses occurred due to shear bands generation which is because of free volume creation in metallic glasses under shear stress. The plastic deformation (shear bands) observation can be done by observing kink angle of metallic glass ribbon samples after bending test.

2) Kink angle measurement helps to understand and characterize the shear bands nature of metallic glasses under different strain rates. At higher strain rate, fewer shear bands generated which gives low kink angle due to higher recovering curvature of ribbon after removal of bending forces and ultimately low plastic deformation, as compared to lower strain rate which has higher plastic deformation which can be recognized by higher kink angle.

3) By extrapolating the relation between kink angle and estimated strain rate to kink angle initiation point (shear band initiation point) we can easily estimate the yield point of metallic glasses.

4) Kink angle measurement also helps to evaluate the nature of shear bands at same strain rate for different metallic glasses. In relatively brittle metallic glass, deformed region is relatively small with local generation of shear bands and higher shear step height, while in relatively ductile metallic glass the deformed region is large with widely spaced shear bands, which cause higher kink angle of brittle metallic glass due to less recovering curvature after bending test as compared to ductile metallic glass which has higher recovering curvature.

5) Kink angle helps to estimate the relative ductility of metallic glasses. As

brittle or strong metallic glass has higher kink angle as compared to ductile or fragile metallic glass.

6) Kink angle measurement helps to explain the deformation behavior in Cu-Zr-Al-Y phase separating metallic glasses, which is normally difficult to explain by other methods due to phase separating nature.

7) It was noted that kink angle of Cu-Zr-Al-Y phase separating metallic glass decrease with the addition of yttrium which helps to define that yield point is decreasing with the addition of yttrium in Cu-Zr-Al alloy which can observed by lower hardness and also by lower fatigue strength.

8) The lower kink angle of yttrium based alloys as compared to yttrium free alloy shows that phase separation cause the ductility in metallic glasses which confirmed by nano indentation results due to lower shear strength at pop-in for yttrium based alloys as compared to yttrium free alloy.

9) These results give us not only information on the deformation tendency depending on the deformation variables (strain rate, bending distance…) but also clues to understand the deformation mechanism of various metallic glasses.

References

[1] C. Suryanarayana, A. Inoue, *Bulk metallic glasses,* CRC Press: Boca Raton (2011).

[2] A. Inoue, X.M. Wang, W. Zhang, Developments and applications of bulk metallic glasses, *Rev. Adv. Mater. Sci.*, 18, 1 (2008).

[3] Klement, W., R.H. Willens, P. Duwez, Non-crystalline structure in solidified gold-silicon alloys, *Nature*, 187, 869 (1960).

[4] Christian, J.W., *The theory of transformations in metals and alloys*, Oxford, U.K: Pergamon (2002).

[5] Suryanarayana, C., *Rapid solidification*. *In processing of metals*, (1991).

[6] Anantharaman, T.R., C. Suryanarayana, *Rapidly solidified metals: A technology overview* (1987).

[7] Jacobson, L.A., J. Mckittrick, Rapid solidification processing, *Mater. Sci. Eng.*, R11, 355 (1994).

[8] Akihisa Inoue, Nobuyuki Nishiyama, New bulk metallic glasses for applications as magnetic-sensing, chemical, and structural materials, *MRS BULLETIN*, 32 (2007).

[9] Peter K. Liaw, New fatigue behavior in bulk metallic glasses (BMGs), *Department of Materials Science and Engineering, The University of Tennessee, Knoxville, TN,* 37996 (2011).

[10] W.H. Wang, C. Dong, C.H. Shek, Bulk metallic glasses, *Materials Science and Engineering*, R 44, 45 (2004).

[11] C. A. Angell, Formation of glasses from liquids and biopolymers, *SCIENCE,* 267 (1995).

[12] Senkov, O.N., Correlation between fragility and glass forming ability of metallic alloys, *Phys. Rev.*, B 76, 104202 (2007).

[13] Zheng, Q., J. Xu, E. Ma, High glass-forming ability correlated with fragility of Mg-Cu (Ag)-Gd alloys, *J. Appl. Phys.*, 102, 113519 (2007).

[14] Inoue, A., T. Shibata, T. Zhang, Effect of additional elements on glass transition behavior and glass formation tendency of Zr-Al-Cu-Ni alloys, *Mater. Trans.*, JIM 36, 1420 (1995).

[15] Porter, D.A., K.E. Easterling, M.Y. Sherif, *Phase transformations in metals and alloys*, CRC Press, 3rd edn., Boca Raton, Fl (2009).

[16] Chen, H.S., D. Turnbull, Formation, stability and structure of palladium-silicon based alloy glasses, *Acta Metall.*, 17, 1021 (1969).

[17] E.S. Park, D.H. Kim, Phase separation and enhancement of plasticity in Cu–Zr–Al–Y bulk metallic glasses, *Acta Materialia* 54, 2597 (2006).

[18] George E. Dieter, *Mechanical metallurgy*, SI Metric Edition.

[19] Na Young Kim, Correlation between fatigue behavior of metallic glass and electrical resistivity change, M.S. Defense, *RIAM, Dept. of Materials Science and Engineering*, Seoul National University (2012).

[20] Eun Soo Park, Dynamic behavior of shear bands in metallic glasses, *Material Science Seminar* (2008).

[21] J.X. Zhao, F.F. Wu, Z.F. Zhang, Analysis on shear deformation mechanism of metallic glass under confined bending test, *Materials Science and Engineering A*,527, 6224 (2010).

[22] Qiang He, Jian Xu, Locating malleable bulk metallic glasses in Zr-Ti-Cu-Al alloys with calorimetric glass transition temperature as an indicator, *J.*

Mater. Sci Technol., 28, 1109 (2012).

[23] Weihong Fu, Yajuan Sun, Wei Zhang, The effect of cooling rate on microstructure and mechanical properties of Zr-based bulk metallic glasses, *Advances in Materials Science and Engineering* (2013).

[24] Henry J. Neilson, Alex S. Petersen, Andrew M. Cheung, S. Joseph Poon, Gary J. Shiflet, Mike Widom, John J. Lewandowski, Weibull modulus of hardness, bend strength, and tensile strength of Ni-Ta-Co-X metallic glass ribbons, *Materials Science & Engineering A,* 634, 176 (2015).

[25] S. Vincent, Joysurya Basu, B.S. Murty, Jatin Bhatt, Micro indentation study on $Cu_{60}Zr_{20}Ti_{20}$ metallic glass, *Materials Science & Engineering A,* 550, 160 (2012).

[26] Devinder Singh, Dharmendra Singh, T. P. Yadav, R. K. Mandal, R. S. Tiwari, O. N. Srivastava, Synthesis and indentation behavior of amorphous and nanocrystalline phases in rapidly quenched Cu–Ga–Mg–Ti and Cu–Al–Mg–Ti alloys, *Metallogr. Microstruct. Anal.*, 2, 321 (2013).

[27] R. D. Conner, W. L. Johnson, N. E. Paton, W. D. Nix, Shear bands and cracking of metallic glass plates in bending, *JOURNAL OF APPLIED PHYSICS,* 94 (2003).

[28] A. Ince, G. Glinka, A modification of Morrow and Smith–Watson–Topper mean stress correction models, *Fatigue & Fracture of Engineering Materials & Structures,* 34, 854 (2011).

[29] Adam Niesłony, Chalid el Dsoki, Heinz Kaufmann, Peter Krug, New method for evaluation of the Manson–Coffin–Basquin and Ramberg–Osgood equations with respect to compatibility, *International Journal of Fatigue,* 30, 1967 (2008).

[30] E. P. Barth, F. Spaepen, R. Bye, S. K. Das, Influence of processing on the ductile-to-brittle transition temperature of an Fe-B-Si metallic glass, *Acta*

mater., 45, 423 (1997).

[31] Wei Hua Wang, The elastic properties, elastic models and elastic perspectives of metallic glasses, *Progress in Materials Science* (2011).

[32] W.H. Wang, C. Dong, C.H. Shek, Bulk metallic glasses, *Materials Science and Engineering R*, 44, 45 (2004).

[33] M. Stoica, J. Eckert, S. Roth, Z.F. Zhang, L. Schultz, W.H. Wang, Mechanical behavior of $Fe_{65.5}Cr_4Mo_4Ga_4P_{12}C_5B_{5.5}$ bulk metallic glass, *Intermetallics*, 13, 764 (2005).

[34] M. Calin, J. Eckert, L. Schultz, Improved mechanical behavior of Cu–Ti-based bulk metallic glass by in situ formation of nanoscale precipitates, *Scripta Materialia*, 48, 653 (2003).

[35] Weidong Li, H. Bei, Y. Tong, W. Dmowski, Y. F. Gao, Structural heterogeneity induced plasticity in bulk metallic glasses: From well-relaxed fragile glass to metal-like behavior, *Applied Physics Letters*, 103, 171910 (2013).

[36] Yuting Li, Deformation behavior of bulk metallic glasses and high entropy alloys by nanoindentation, *Master thesis*, The University of Tennessee, Knoxville (2013).

[37] Yoshihiko Yokoyama, Hitoo Tokunaga, Alain Reza Yavari, Toru Kawamata, Tohru Yamasaki, Kazutaka Fujita, Kazumasa Sugiyama, Peter K. Liaw, Aakihisa Inoue, Tough hypoeutectic Zr-based bulk metallic glasses, *Metallurgical and Materials Transaction A*, 42A, 1468 (2011).

[38] Che-Nan Kuo, Microstructural and mechanical response of CuZrAl-V/Co bulk metallic glass composites, *Doctorate Dissertation*, National Sun Yat-sen University (2013).

[39] G.Y. Wang, P.K. Liaw, A. Peker, B. Yang, M.L. Benson, W. Yuan, W.H.

Peter, L. Huang, M. Freels, R.A. Buchanan, C.T. Liu, C.R. Brooks, Fatigue behavior of Zr–Ti–Ni–Cu–Be bulk-metallic glasses, *Intermetallics,* 13, 429 (2005).

[40] Yoshihiko Yokoyama, Kenzo Fukaura, Akihisa Inoue, Effect of Ni addition on fatigue properties of bulk glassy $Zr_{50}Cu_{40}Al_{10}$ alloys, *Materials Transactions,* 45, 1672 (2004).

[41] Yoshihiko Yokoyama, Kenzo Fukaura, Hisakichi Sunada, Fatigue properties and microstructures of $Zr_{55}Cu_{30}Al_{10}Ni_5$ bulk glassy alloys, *Materials Transactions, JIM,* 41, 675 (2000).

[42] Byoung-Joon Kim, Hae-A-Seul Shin, Sung-Yup Jung, Yigil Cho, Oliver Kraft, In-Suk Choi, Young-Chang Joo, Crack nucleation
during mechanical fatigue in thin metal films on flexible substrates, *Acta Materialia,* 61, 3473 (2013).

[43] G.Y. Wang, P.K. Liaw, M.L. Morrison, Progress in studying the fatigue behavior of Zr-based bulk-metallic glasses and their composites, *Intermetallics,* 17, 579 (2009).

[44] G.Y. Wang, P.K. Liaw, A. Peker, M. Freels, W.H. Peter, R.A. Buchanan, C.R. Brooks, Comparison of fatigue behavior of a bulk metallic glass and its composite, *Intermetallics,* 14, 1091 (2006).